INTERNATIONAL JOURNAL FOR NUMERICAL AND ANALYTICAL METHODS IN GEOMECHANICS, VOL. 22, 351–391 (1998)

DIMENSIONLESS AND UNBIASED CPT INTERPRETATION IN SAND

DAWN SHUTTLE[1] AND MICHAEL JEFFERIES[2,*]

[1] *Golder Associates Inc, Redmond, Washington, U.S.A.*
[2] *Golder Associates (U.K.) Ltd., Landmere Lane, Edwalton, Nottingham, NG12 4DG, U.K.*

SUMMARY

The cone penetration test (CPT) is widely used, and although initially developed as a stratigraphic logging tool its excellent repeatability and accuracy offers a benchmark quantitative test for sand in particular. A continuing difficulty, however, is that the CPT does not measure any soil property directly, so that parameters of interest must be recovered from solution of an inverse boundary value problem, which is difficult. To date most CPT interpretations in sand have been based on very limited calibration testing carried out in large chambers on a few sands from which mappings are developed. But there are differences in the CPT response from one sand to another leaving the interpretation imprecise (and arguably even speculative) because these differences remain poorly understood. In this paper we use the familiar spherical cavity expansion analogy to the CPT including large strains and a good, critical-state-based, soil model to develop a pattern of behaviour which we then compare to some of the reference chamber test data. We find that one of the issues of dispute in the empirical interpretation methods, the so-called stress-level effect, is caused by neglect of elasticity and that there are several additional parameters of first-order significance to cavity expansion in sands. More generally, we show that the difference in CPT response between various chamber sands in predicted. Our results are cast in dimensionless form and the inversion illustrates that extreme care is required in interpreting CPT data if the *in situ* sand state is to be determined with precision approaching that suggested as achievable by the repeatability of the CPT data itself. Aspects requiring particular care in interpreting CPT data in sand are discussed. © 1998 John Wiley & Sons, Ltd.

Int. J. Numer. Anal. Meth. Geomech., vol. 22, 351–391 (1998)

Key words: cone penetration testing; sand

INTRODUCTION

Geotechnical engineering of sands largely depends on penetration tests because of the difficulty in sampling sands in anything like an undisturbed condition. A considerable cone penetration test (CPT) industry has developed world wide, with many specialist contractors testing hundreds of thousands of metres of sounding per year. The particular advantage of the CPT is the interesting combination of a continuous data record with excellent repeatability and accuracy at relatively low cost. Although it might be argued that original interest in the CPT derived from the geologic perspective of stratigraphic identification using the continuous record, more recently it is the unusual repeatability and accuracy of the test that is attracting attention from the geomechanics

Correspondence to: M. Jefferies, Golder Associates (U.K.) Ltd., Landmere Lane, Edwalton, Nottingham, NG12 4DG, U.K.

CCC 0363–9061/98/050351–41$17.50

Received 5 July 1996
Revised 5 September 1997

perspective: the CPT offers a determination of penetration resistance to an accuracy of typically better than 2 per cent (see ASTM standard D3441) which is unusually precise for soil testing.

Despite the accuracy and repeatability of the CPT, uncertainty surrounds the quantitative use of CPT data. Uncertainty arises because the CPT presents an inverse boundary value problem requiring interpretation of data to obtain the parameters of interest. Currently, most interpretation of the CPT in sand is based on large calibration chamber (CC) testing in which CPT response is measured under controlled conditions to develop a mapping between response and some combination of sand density and stress. But, there is no unique mapping applicable to all sands and only a few sands have been tested.

The consequence of the absence of a universal mapping is best understood by example. Hilton Mines sand at 60 per cent relative density produces the same CPT resistance as Monterey sand at 40 per cent relative density all other factors remaining equal (see Figure 4 of Robertson and Campanella): in many circumstances a 40 per cent relative density will be regarded as inadequate while 60 per cent could well be acceptable. When dealing with a different sand, is that sand to be regarded as more like Hilton Mines or Monterey? And, why? And what happens if it is not like either? The entire engineering decision hinges on nuances attached to unquantified factors unrelated to the CPT data itself. In short, the promise implied by the repeatability of the CPT is not being delivered to the end user as reliable engineering parameters and it would not be unreasonable to characterize most CPT interpretation as speculative.

Mechanics has been limited in its contribution to the CPT because the CPT is a difficult problem: penetration is essentially a continuous flow situation with a high degree of confinement, and the soil goes from at rest conditions to the critical state. Reasonable understanding can only emerge from large strain analysis with a good soil model. Such good soil models are not analytically tractable.

In this paper, we approximate the CPT as an expansion of a spherical cavity and analyse the expansion of the cavity to large displacement using a good soil model. The approach is numerical, and such simulations show how the CPT is affected by those properties of sand readily and reliably measured in conventional triaxial testing on reconstituted samples. We then invert a dimensionless form of the numerical results to illustrate the elements of a universal CPT interpretation methodology founded in mechanics.

The numerical results are compared with calibration test data for the CPT in two laboratory reference sands: Ticino and Hilton Mines. Ticino was chosen as it has been extensively investigated and there is a considerable body of data on both the properties of the sand and the response of the CPT under a range of initial conditions. Hilton Mines was selected because it is a sand that misfits empirically derived 'universal' CPT interpretation methodologies (e.g. Reference 2) and so is a good test of the proposed approach based on consistent mechanics.

As our interest is drained cavity expansion, all stresses are taken as effective throughout this paper.

BACKGROUND TO CPT INTERPRETATION IN SAND

A CPT in sand provides just two signals, the tip resistance and the sleeve friction (the penetration is drained so the pore pressure transducer simply measures hydrostatic pore pressure). Only two independent parameters (at most) can be deduced from CPT data in sand. Which is why most CPT data are interpreted in terms of one parameter alone, commonly relative density, but sometimes peak friction angle. Interpreting CPT data while constrained by this fundamental

mathematical limitation requires a good representation of a sand's constitutive behaviour in terms of some *in situ* state index (which is to be measured by the CPT) and a few material properties that can readily be established by testing disturbed samples.

Relative density is an almost universally used state index for sand. However, it is easy to show with a modest laboratory test program that it is misleading. It is well known that dilatancy can be suppressed by mean stress. In addition, when dealing with sands with a few per cent silt, one mixture at 40 per cent relative density can dilate while another mixture at 60 per cent relative density can be contractive.[3] There are two alternatives which avoid these errors: the relative dilatancy index[4] and the state parameter approach.[3] Work to date with the CPT has used the state parameter.

The state parameter, ψ, is simply defined as the difference between the void ratio in the current state and that at the critical state for the same mean stress (see Figure 1). A wide range of constitutive models can be developed around this basic idea of a material independent state parameter.[5–7] Because ψ is used as a state variable in these models, the subscript '0' is used to denote the *in situ* (or initial) value of ψ under geostatic conditions to be consistent with the original usage by Been and Jefferies.[3]

Initial work with determining ψ from CPT data comprised triaxial testing of the various sands for which chamber test data was available to define the critical state locus (CSL) of each

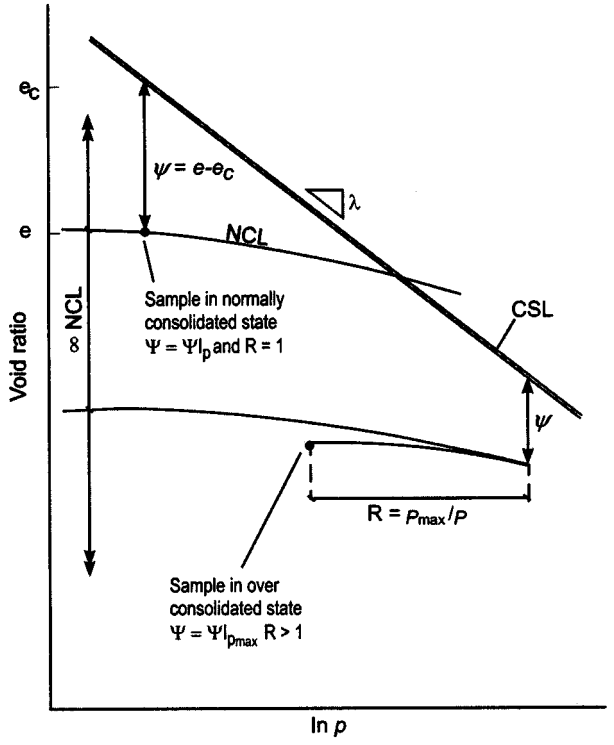

Figure 1. Definition of ψ and the concept of an infinity of NCL

sand and then processing the chambers test data to develop dimensionless relationships[2,8] in the form

$$Q = k\exp(-m\psi_0) \tag{1}$$

The two coefficients in (1) differ from one sand to another, and it was suggested that both coefficients were functions of the slope of the CSL, λ.

The framework of Been *et al.*[2,8] is not without its problems however. Sladen[9,10] suggested that ψ_0 determined from (1) was biased by stress level with potential errors of as much as $\Delta\psi = \pm 0{\cdot}2$. The significance of this bias can be noted from the range in values for ψ. At the dense end of the spectrum, sands will rarely be encountered denser than $\psi_0 < -0{\cdot}3$. Conversely, even the most statically liquefiable sands are rarely looser than $\psi_0 > 0{\cdot}05$. Thus, the suggested bias because of stress level was in the order of 50 per cent of the credible range in the parameter sought.

The expansion of spherical cavities has been used to idealize penetration processes in soil for some 50 years. The initial work by Bishop *et al.*[11] and Hill[12] addressed incompressible materials with associated flow rules, corresponding to the familiar and simple idealization of the undrained behaviour of clay. Chadwick[13] derived the pressure–expansion relationship for a Mohr–Coulomb material with an associated flow rule, and the interesting further development of cavity expansion theory for non-associated flow has been considered by a number of workers including Carter *et al.*[14] and Yu and Houlsby[15]. The central assumption of these studies has been that both the friction and dilation angles remain constant during shear. Although this assumption leads to straightforward expressions with analytical or semi-analytical solutions, the assumption has the fundamental deficiency that soil does not behave in such a manner and cavity expansion is a problem in which the nuances of soil behaviour are of first-order significance to the solution. Reliable solutions require a stress–strain model that captures the evolution of dilatancy with accumulated strain and stress, as it is this behaviour that distinguishes one sand from another and is magnified by the confinement of the cavity expansion.

In the development of reliable solutions for drained cavity expansion, Collins *et al.*[5] made an important contribution using a state-parameter-based numerical analysis. The results of Collins *et al.* showed that there was an effect of stress level on the state parameter approach, consistent with the suggestion of Sladen, and further that the relationship between Q and ψ_0 depended on material properties of the sand. However, Collins *et al.* did not develop their approach into a general framework of CPT interpretation: it is unclear how their computed interpretation coefficients are related to what could be easily measured in a triaxial test (or the like). Subsequently, Jefferies and Been[16] compared the Collins *et al.* results for Ticino 4 sand (a standard Italian test reference sand used in CC work) and found that the computed effect of stress level was half the experimental scatter in the CC data.

Although it is the stress level issue that has attracted attention, by far the weakest point in (1) is the suggested dependence of the two parameters k, m on λ alone, as this suggestion is based on neither numerics nor theory but speculative association based on λ controlling plastic hardening in standard critical state soil mechanics.[17] Our goal then is to remedy this deficiency by finding a function C, based on comprehensive numerical studies, such that

$$\psi_0 = C(q_c, G, p, \dots) \pm 0{\cdot}01 \tag{2}$$

where the terms in C are either those directly and easily measured *in situ* (q_c, G) or determined by testing of reconstituted samples using routine laboratory procedures. Of course, better accuracy

would be desirable but the CC reference data has significant experimental scatter and it is unrealistic to expect better than $\Delta\psi = 0{\cdot}01$.

THE NORSAND CONSTITUTIVE LAW

Description

NorSand[6] is an isotropically-hardening-isotropically-softening, single-yield-surface plastic model for sand that produces realistic dilation rates despite the assumption of normality. NorSand was derived from two axioms of critical state theory:

(i) a CSL exists (the first axiom).
(ii) soil state moves to the CSL with shear (the second axiom).

The first of these axioms has been discussed by many workers and a detailed experimental investigation was presented by Been *et al.*[18] Importantly, note that a principal source of error in the past, and continuing quite widely, arises through the definition that the critical state is the condition in which the soil deforms without volume change, otherwise expressed as zero dilatancy. While this is a necessary condition, it is not sufficient for criticality. At a critical state there must also be the condition that the rate of change of dilatancy is zero for constant mean stress (see Reference 6 for a formal and unambiguous definition of the CSL).

It is conventional to describe the CSL in e–p space using the semi-logarithmic form

$$e_c = \Gamma - \lambda \log(p_c) \tag{3}$$

where Γ, λ are material properties (constants). The validity of (3) at low mean stress has been discussed in the literature,[19] but objections to the range of applicability of (3) are merely arguments about detail. NorSand is properly defined for any single-valued function for the CSL in e–p space. We will keep the classical form (3) for the present.

Standard critical state models (e.g. CamClay) assume that any yield surface intersects the CSL thus directly coupling the yield surface size to void ratio. Real soils, however, display a far richer behaviour and, in particular, exhibit an infinity of normal consolidation loci (NCL) which are not parallel to the CSL. It is this rich behaviour that is characterized by the state parameter approach, in essence each NCL being related to a value of ψ. Overconsolidation ratio (R) continues to exist in its usual sense of defining the location of a stress state within a yield locus (see Figure 1).

NorSand adopts Nova's flow rule[20] which is (for the triaxial conditions of interest with spherical cavity expansion):

$$D = (M - \eta)/(1 - N) \tag{4}$$

where M, N are material constants. The yield surface is then obtained in the usual manner of critical-state theory by assuming normality and integrating the flow rule. For the case of $N \neq 0$ (see Reference 6 for the full equation set), this then gives

$$\eta = \frac{M}{N}\left[1 + (N-1)\left(\frac{p}{p_i}\right)^{N/(1-N)}\right] \tag{5}$$

where p_i is a parameter with the dimension of stress that sizes the yield surface. The subscript i denotes the image state and it is the concept of image conditions that is central to NorSand. The

idea of an image state arises because, in general, yield surfaces do not intersect the critical state. Recall that for criticality not only must (3) be satisfied but also

$$q = Mp_c \tag{6}$$

where the subscript c denotes that p_c lies on the CSL, here defined by (3). The image stress, p_i, is defined by analogy to (6) but without the linkage to (3) (see Figure 2) and has the effect that any soil at its image states meets one of the two mathematical conditions for criticality. The second axiom of critical state theory is then satisfied by requiring that the image state evolves to critical:

$$p_i \Rightarrow p_c \quad \text{as } \varepsilon_q \Rightarrow \infty \tag{7}$$

Eventually this drives NorSand yield surfaces to intersect the CSL. Equation (7) is a generalization of a hardening law.

Support for the idea of an infinity of NCL is given on Figure 3 which plots the isotropic compression of Erksak sand from several initial void ratios in comparison with the CSL (established for this Erksak sand by undrained triaxial shear[18]). Each isotropic compression line

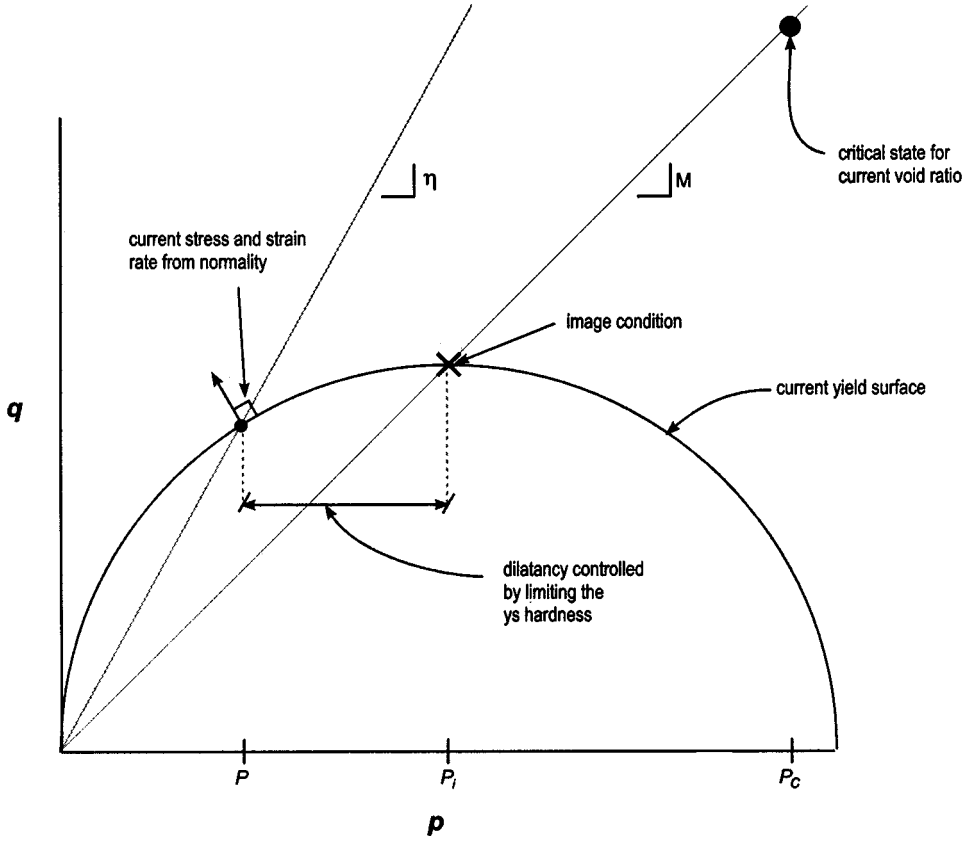

Figure 2. Definition of image state on yield surface

is a NCL as substantiated by two factors. First, the samples were prepared under low stresses (some by gentle moist tamping, some by pluviation) and never overconsolidated. Second, the unload–reload loops define a classic elastic–plastic form, as illustrated in the expanded view on Figure 3, and including in particular samples denser than the CSL.

Within this framework of an infinity of NCL, there is a corresponding dissociation of the yield surface from the CSL in general. Hardening of the yield surface is derived from the Second Axiom but constrained to give realistic dilation rates by limiting the maximum size of the yield surface. This is done by limiting p_i to a maximum value (i.e. strictly applying the concepts of Drucker *et al.*[21]), computed from the relation:

$$\left(\frac{p_{i,\max}}{p}\right) = \left(1 + 3{\cdot}5\Psi_i \frac{N}{M}\right)^{(N-1)/N} \tag{8}$$

and from which the yield surface hardening then follows as

$$\frac{\dot{p}_i}{p_i} = 2{\cdot}718, H \exp\left(-\frac{\eta}{M}\right)\left(\frac{p_{i,\max}}{p_i} - 1\right)\dot{\varepsilon}_q \tag{9}$$

Notice that within NorSand ψ is used as a rate variable so that we have what amounts to a differential form of classic critical state models (CamClay can be recovered as a special case of NorSand).

Elastic strains also exist in sand. We use isotropic elasticity with a constant Poisson's ratio, v, and shear modulus, G. Test data suggests that, while v can be treated as a constant, G is a function of both void ratio and stress in sands. Several workers have studied the relationship between elasticity, void ratio and stress including Richart *et al.*,[22] Pestana and Whittle[23] and Bellotti *et al.*,[24] but there is no consensus on the form of the relationship between these parameters. On the other hand, Collins *et al.* note that using a constant G within a cavity expansion simulation leads to only about a 10 per cent underestimate of the cavity pressure compared to allowing the modulus to increase with the square root of the mean stress. Based on this result, in developing the parametric plots, we have used a constant G within any realization and treated G as an independent parameter that must be measured or otherwise known. For the calibration against Ticino sand, G was set constant within a simulation but also made to depend on the initial conditions of void ratio and stress as reported by Bellotti *et al.*[24] and discussed below. For the calibration against Hilton Mines sand, we have used the same elastic relationship as Ticino sand because there is no test data on Hilton Mine sand itself (the possible consequences of this assumption are discussed later).

NorSand is a sparse model with the variant presented here requiring two more parameters than CamClay: N and H. N is a volumetric coupling parameter (the choice $N = 0$ recovers the CamClay flow rule) and as such acts as a scale factor for the stress–dilatancy relationship. The dimensionless hardening modulus H is required because the state parameter approach decouples the yield surface from the CSL and hence the slope of the CSL in e–$\ln(p)$ space no longer acts as a plastic compliance.

Calibration to Ticino sand

Several sands have been used for CC studies, and one of the most extensively tested is Ticino sand used by the group at the University of Torino[22,25]. To minimize experimental uncertainties,

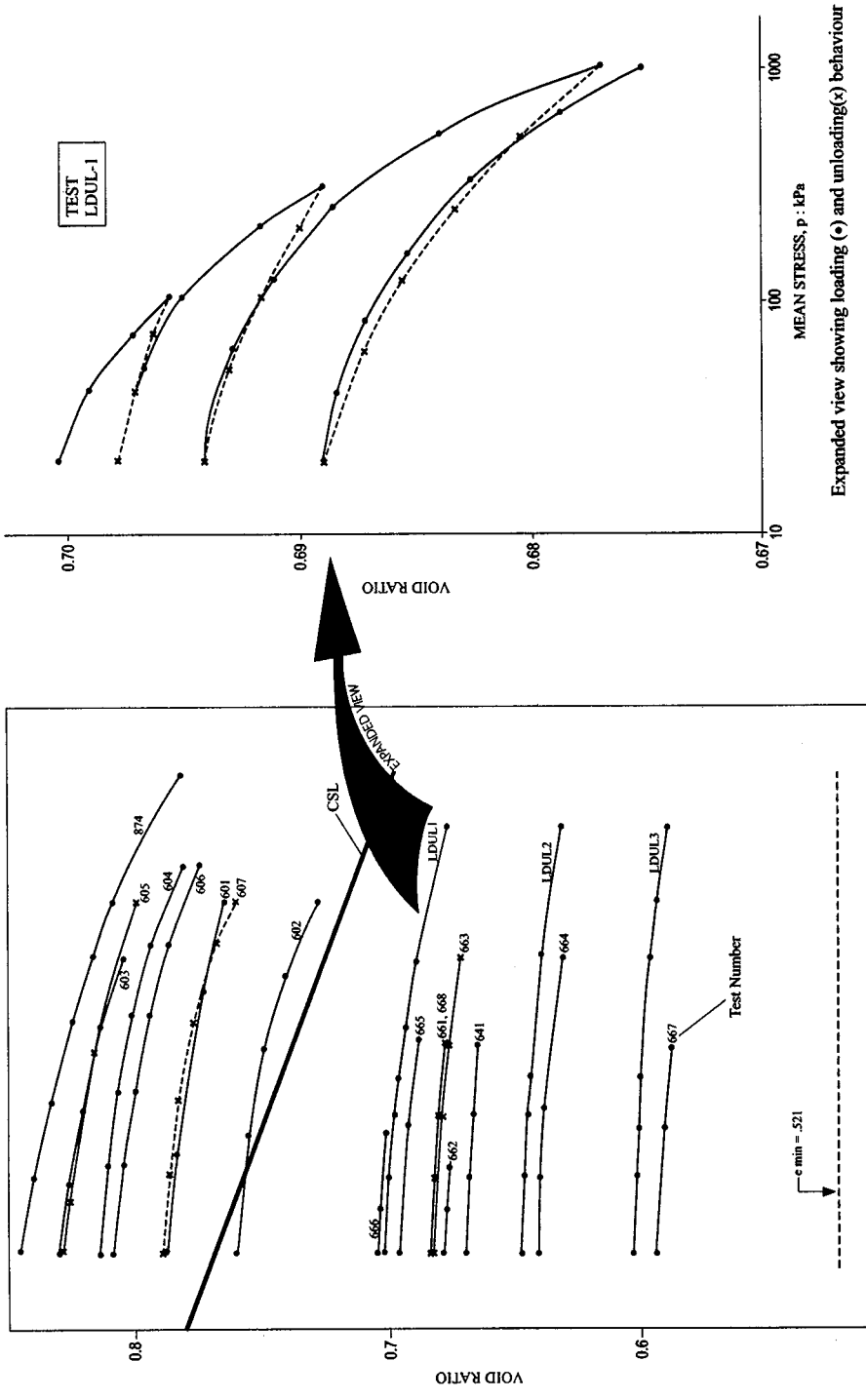

Figure 3. Isotropic compression of Erksak 330/0·7 sand

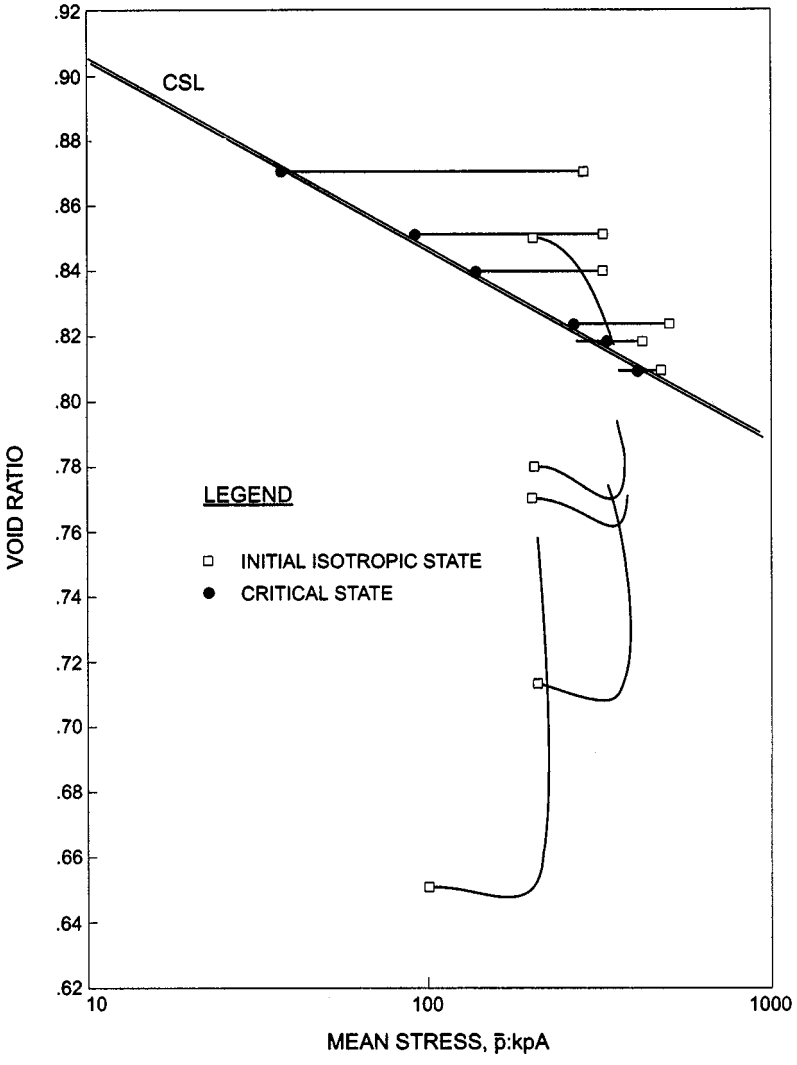

Figure 4. State paths for triaxial tests on Ticino sand showing determination of CSL

we have selected one subject of this testing for the calibrations considered here. This subset is known as Ticino 4 sand, subsequently simply called Ticino sand.

Samples of Ticino sand were obtained and tested in undrained triaxial compression (6 tests) to define the CSL, and in drained triaxial compression (5 tests) to provide other calibration data. Figure 4 shows the state diagram for the test program, including the CSL determined from it. This test program was previously reported in summary form by Been *et al.*[2]

Bellotti *et al.*[24] reported an extensive test program on the elasticity of Ticino sand, mainly investigating the cross-anisotropic elasticity. For the present purpose in which we use a simpler isotropic approximation, their data can be averaged and fitted with the same form of functional

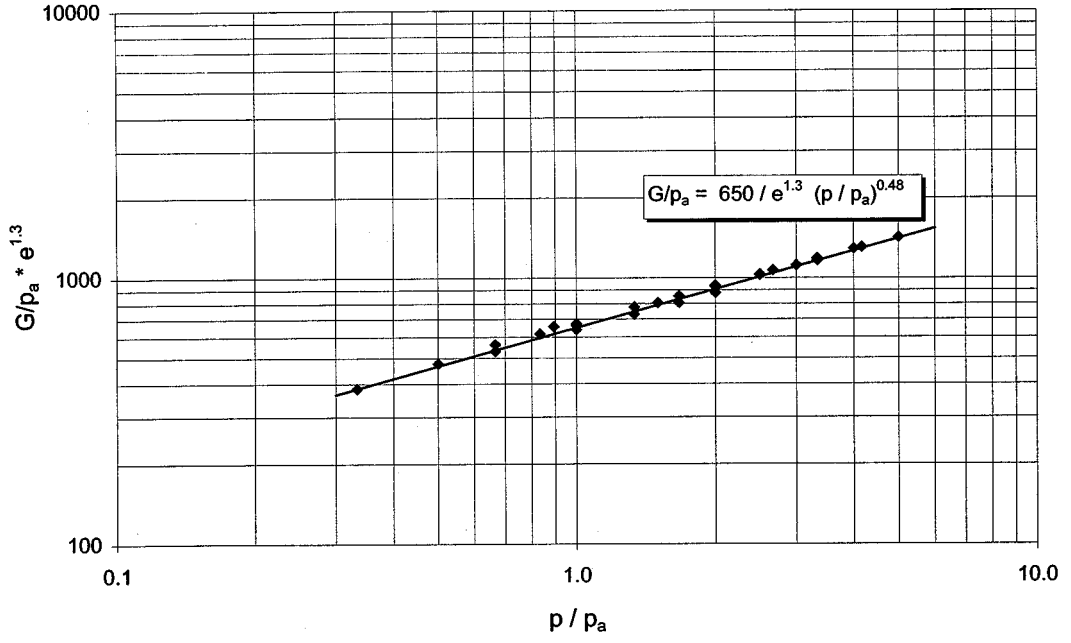

Figure 5. Elastic shear modulus for Ticino sand

Table I. NorSand Parameters for two CPT chamber sands

Parameter	Ticino 4	Hilton Mines	Remark
Γ	0·962	1·315	Defined at 1 kPa
λ	0·0248	0·0738	Defined on base e
M	1·23	1·39	In compression
N	0·2	0·2	
H	$115–420\Psi_0$	$\approx 65\ \forall\psi_0$	See Figure 8 for Ticino
G	30–80 MPa	30–80 MPa	Equation (10)
v	0·2	0·2	

dependence on void ratio and mean stress as they propose, illustrated in Figure 5. This gives the following expression for G:

$$G = \frac{65}{e^{1\cdot3}}\left(\frac{p}{p_a}\right)^{0\cdot48} \tag{10}$$

where G given by (10) has units of MPa and p_a is atmospheric pressure. The elastic bulk modulus was computed from (10) assuming $v = 0\cdot2$ which is consistent with the data reported by Bellotti *et al.*[21]

NorSand parameters for Ticino sand were determined by modelling the drained triaxial tests and selecting the parameter set that gave the best overall fit across all five drained tests. Figures 6 and 7 show the fit between model and data for the loosest and the densest tests, respectively. Based on the fits to triaxial test data the plastic hardening modulus H is clearly a strong function of ψ_0, see Figure 8, but other parameters remain constant. The parameter set representing Ticino sand is summarized in Table I.

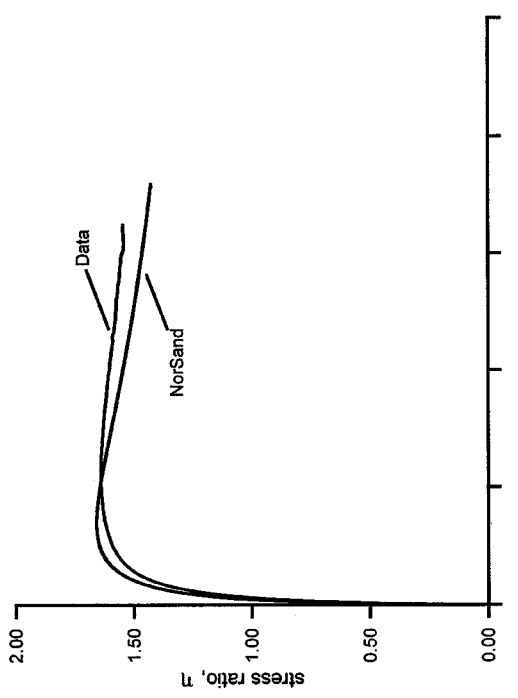

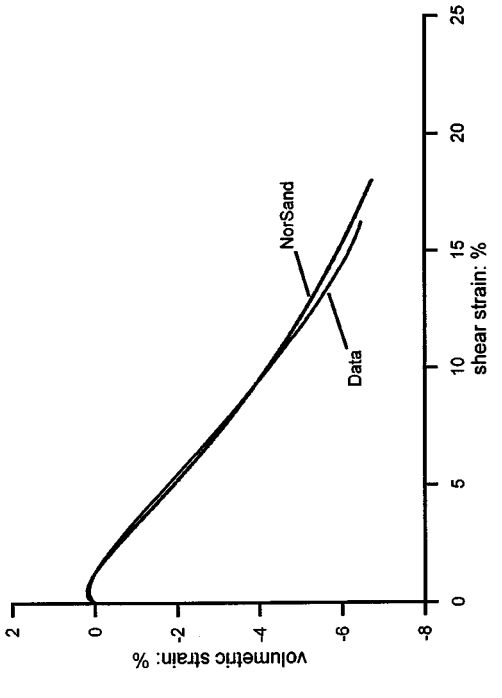

Figure 7. Fit of NorSand to very dense Ticino sand (test cid_265)

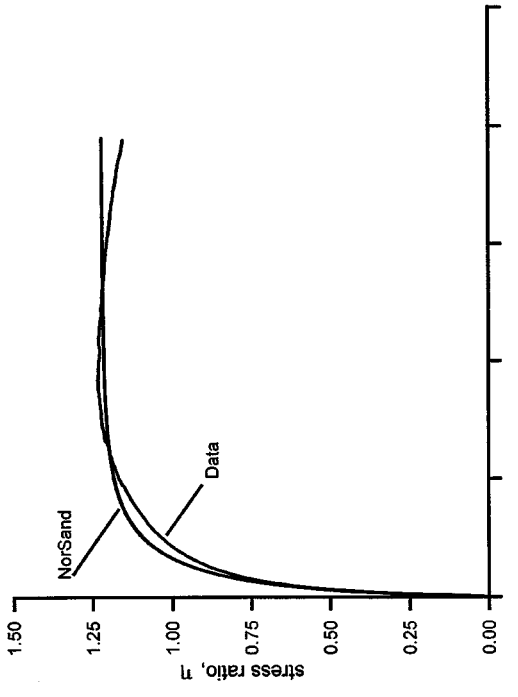

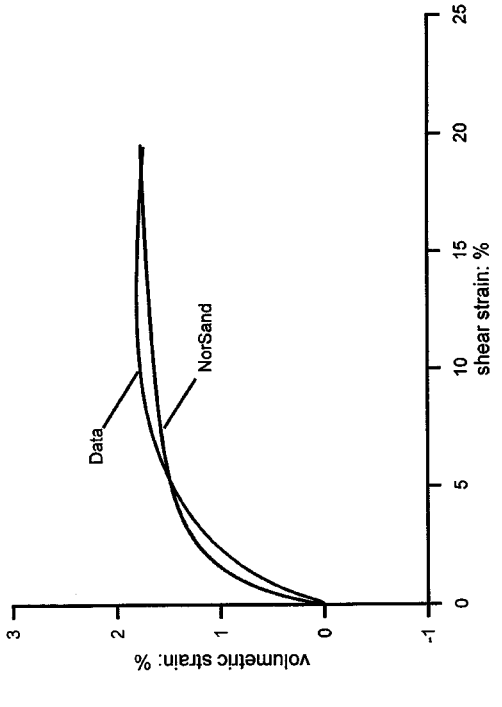

Figure 6. Fit of NorSand to very loose Ticino sand (test cid_262)

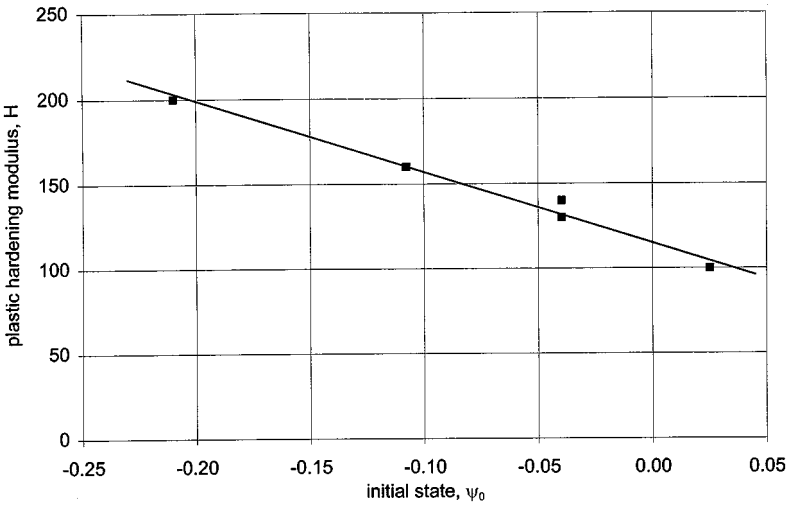

Figure 8. Effect of initial state on shear hardening modulus for Ticino sand

Calibration to Hilton mine sand

The calibration of NorSand to Hilton Mine sand followed the same procedure as discussed for Ticino sand, and also uses the test data of Been *et al.*[2] The laboratory testing included undrained triaxial compression (6 tests) to define the CSL and drained triaxial compression (6 tests) to derive the other parameters.

Unlike Ticino sand, however, there are no measurements of elasticity in Hilton Mine sand. The isotropic elastic model from Ticino sand was therefore assumed to fit Hilton Mine sand as well. This then allowed NorSand parameters to be established by again fitting the triaxial test data, an example of the fit being shown on Figure 9 for a strongly dilating sample. There is an excellent fit but this may be obscuring two compensating errors: too stiff elasticity and too soft plasticity (or the opposite). Interestingly, no dependence of H on ψ_0 was apparent in the Hilton Mine test data, unlike the Ticino sand shown on Figure 8.

The parameter set representing Hilton Mine sand is also summarized on Table I.

NUMERICAL FORMULATION FOR SPHERICAL CAVITY

The NorSand triaxial and spherical analyses were carried out using a large strain viscoplastic finite element code. The numerical approach was conventional. The incremental viscoplastic formulation[26] was implemented using the general approach described in Reference 27 and presented in more detail in Reference 28. A flow chart illustrating the solution methodology, including the viscoplastic formulation, is given in Appendix II.

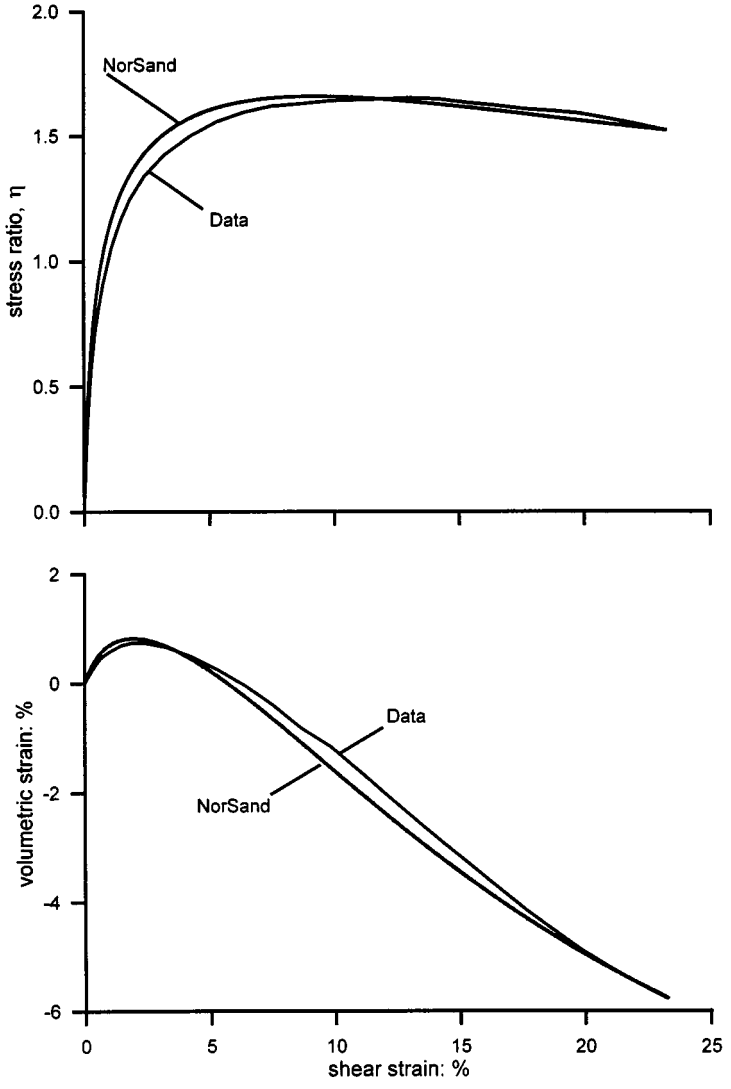

Figure 9. Fit of NorSand to dense Hilton Mine sand (test hm_O261)

Large-strain analysis

The large-strain formulation may most conveniently be understood by first presenting the components of strain used in the analyses, and describing how they are calculated within the code.

The total Green strain ε is considered to be comprised of the standard Cauchy small strain, ε_S, and a large-displacement component, ε_L, such that

$$\varepsilon = \varepsilon_S + \varepsilon_L \tag{11}$$

which for the spherical geometry used in these analyses may be written as

$$\begin{Bmatrix} \varepsilon_r \\ \varepsilon_{\theta 1} \\ \varepsilon_{\theta 2} \end{Bmatrix} = \begin{Bmatrix} -\dfrac{\partial u}{\partial r} \\ -\dfrac{u}{r} \\ -\dfrac{u}{r} \end{Bmatrix} + \frac{1}{2} \begin{Bmatrix} \left(-\dfrac{\partial u}{\partial r}\right)^2 \\ \left(-\dfrac{u}{r}\right)^2 \\ \left(-\dfrac{u}{r}\right)^2 \end{Bmatrix} \tag{12}$$

u being the radial displacement at radius r.

The Cauchy small-strain increment is computed in the standard way using

$$\mathrm{d}\varepsilon_s = B\,\mathrm{d}a \tag{13}$$

where da is the incremental nodal displacement. The non-linear shape functions developed by Yu[29] were used to define the elastic displacement field. These shape functions define the displacement interpolation function for spherical expansion to be

$$u = \frac{C_0}{r^2} + C_1 r \tag{14}$$

For near incompressible materials the displacement field around the cavity takes the form $u = C/r^2$, where C is constant and r is the radial distance. These shape functions are able to reproduce this behaviour exactly, whereas linear interpolation functions are not,

For the shape functions used the B matrix reduces to

$$B = \begin{bmatrix} \dfrac{2R_1^2R_2^3}{r^3\mathrm{RR}} + \dfrac{R_1^2}{\mathrm{RR}} & -\dfrac{2R_1^3R_2^2}{r^3\mathrm{RR}} - \dfrac{R_2^2}{\mathrm{RR}} \\ -\dfrac{R_1^2R_2^3}{r^3\mathrm{RR}} + \dfrac{R_1^2}{\mathrm{RR}} & \dfrac{R_1^3R_2^2}{r^3\mathrm{RR}} - \dfrac{R_2^2}{\mathrm{RR}} \\ -\dfrac{R_1^2R_2^3}{r^3\mathrm{RR}} + \dfrac{R_1^2}{\mathrm{RR}} & \dfrac{R_1^3R_2^2}{r^3\mathrm{RR}} - \dfrac{R_2^2}{\mathrm{RR}} \end{bmatrix} \tag{15}$$

where r is the radius at the stress sampling location, L the element length, $R_1 = r - L/2$, $R_2 = r + L/2$ and $\mathrm{RR} = R_2^3 - R_1^3$.

Further,

$$\mathrm{d}\varepsilon_{\mathrm{L}} = B_L\,\mathrm{d}a \tag{16}$$

By inspection it can be seen that the large-strain component of (12) could be presented as

$$\varepsilon_{\mathrm{L}} = \frac{1}{2} \begin{bmatrix} -\dfrac{\partial u}{\partial r} & 0 & 0 \\ 0 & -\dfrac{u}{r} & 0 \\ 0 & 0 & -\dfrac{u}{r} \end{bmatrix} \begin{Bmatrix} -\dfrac{\partial u}{\partial r} \\ -\dfrac{u}{r} \\ -\dfrac{u}{r} \end{Bmatrix} \tag{17}$$

or

$$\varepsilon_{\mathrm{L}} = \tfrac{1}{2}\,[A]\{\theta\} \tag{18}$$

Which may conveniently be rewritten as

$$\mathrm{d}\varepsilon_{\mathrm{L}} = \tfrac{1}{2}\,\mathrm{d}A\,\theta + \tfrac{1}{2}A\,\mathrm{d}\theta = A\,\mathrm{d}\theta$$

or by reference to (12) and (13)

$$\mathrm{d}\varepsilon_{\mathrm{L}} = A\,\mathrm{d}\theta = AB\,\mathrm{d}a \tag{19}$$

Hence, equation (19) provides an alternative form to (16).

Returning to the formulation, the large-strain algorithm used for the CPT analysis was implemented by updating the nodal co-ordinates every load increment and incorporating the geometric effect via a convected term added to the geometric stiffness matrix.

Applying this methodology, the total tangential stiffness matrix, K_{T}, may be written as[30]

$$K_{\mathrm{T}} = (K_0 + K_{\mathrm{L}}) + K_\sigma \tag{20}$$

The first two terms of the stiffness matrix, $(K_0 + K_{\mathrm{L}})$, are computed by updating the nodal co-ordinates at the end of every load step; the displacement component of the stiffness matrix is then given by

$$(K_0 + K_{\mathrm{L}}) = \int_V B^{\mathrm{T}}\mathrm{Dee}\,B\,\mathrm{d}V \tag{21}$$

where Dee is the usual elastic axisymmetric stress–strain matrix dependent on the elastic shear modulus, G, and Poisson's ratio, v:

$$\frac{2Gv}{(1-2v)}\begin{bmatrix} \dfrac{(1-v)}{v} & 1 & 1 \\ 1 & \dfrac{1}{2v} & \dfrac{1}{2v} \\ 1 & \dfrac{1}{2v} & \dfrac{1}{2v} \end{bmatrix} \tag{22}$$

and B is the standard small-strain version of the strain–displacement matrix presented in (15), with the nodal co-ordinates being updated every load increment.

The final term in the stiffness matrix, K_σ, is a symmetric matrix dependent on the stress level and known as the *geometric matrix*. The matrix K_σ is given by

$$K_\sigma\,\mathrm{d}a = \int_V \mathrm{d}B_{\mathrm{L}}^{\mathrm{T}}\,\sigma\,\mathrm{d}V \tag{23}$$

where B_L corresponds to the large-strain component of the strain increment. By inspection of equations (16) and (19), $B_L = A.B$, giving

$$K_\sigma \, \mathrm{d}a = \int_V B^T \, \mathrm{d}A^T \sigma \, \mathrm{d}V \tag{24}$$

Now, writing[30]

$$\mathrm{d}A^T \sigma = \begin{bmatrix} \sigma_r & 0 & 0 \\ 0 & \sigma_{\theta 1} & 0 \\ 0 & 0 & \sigma_{\theta 2} \end{bmatrix} \mathrm{d}\theta = M \, \mathrm{d}\theta = MB \, \mathrm{d}a \tag{25}$$

and rearranging equation (24) gives, for the spherical geometry used here

$$K_\sigma = \int_V B^T M B \, \mathrm{d}V \tag{26}$$

The large-strain stiffness matrix is thus constructed by forming the standard stiffness matrix using the updated nodal co-ordinates, and adding an extra expression to account for the convected term.

Verification of viscoplastic integration of NorSand

Viscoplastic solution of work hardening–softening soil models is not widespread. Therefore to confirm that the numerical algorithm was operating correctly for NorSand, conventional triaxial compression tests were modelled. The behaviour computed using direct numerical integration of the NorSand equations was compared with that obtained from the finite element code.

A single four-node element was used, which reduced to two degrees-of-freedom (one vertical displacement and one radial displacement) through symmetry. Linear shape functions were used to remain consistent with the formulation subsequently used for the spherical analyses. A single integration point at the centre of the element was adopted.

The triaxial test was modelled by applying vertical displacement to the top of the element, and calculating the horizational displacement, and vertical, radial and circumferential stresses. The results of the comparison are presented in Figure 10 which shows both the variation of stress ratio and the volumetric strain against the shear strain. There is close agreement between the finite element and the direct integration solutions thus confirming a correct implementation of NorSand within the viscoplastic algorithm.

FINITE ELEMENT ANALYSIS OF SPHERICAL CAVITY EXPANSION

Finite element model

The CPT is idealized as a cavity in an infinite uniform medium under an isotropic stress state p_0, with the internal pressure of the cavity initially equal to the isotropic stress. The cavity is expanded by a monotonically increasing radius until a limiting (constant) pressure is obtained, this being the pressure of interest. As shown in the preceding section, this idealization greatly

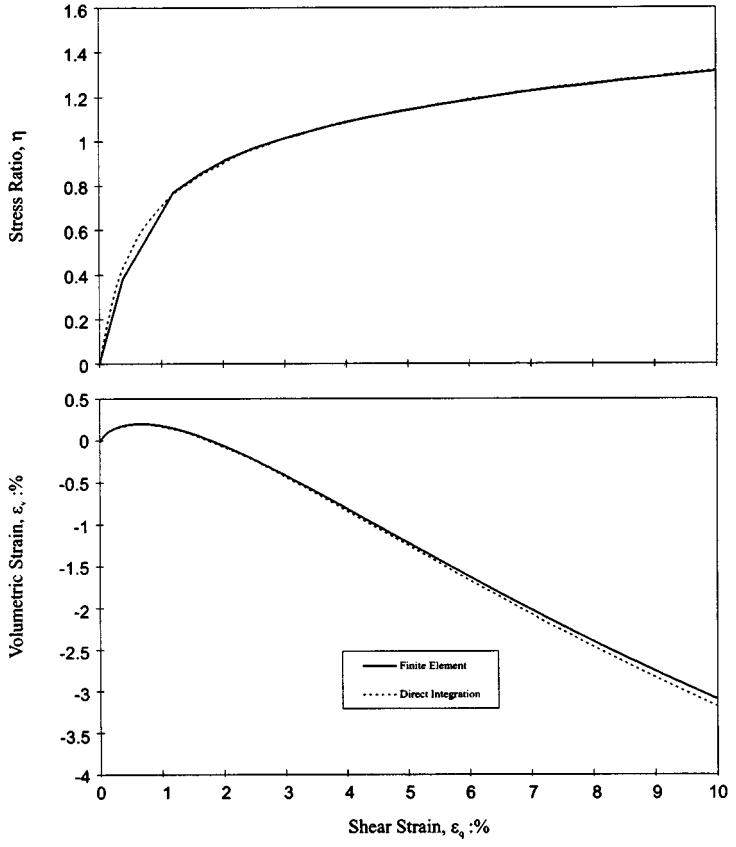

Figure 10. Comparison of viscoplastic finite element solution with direct integration for drained triaxial test

simplifies the analysis because the spherical symmetry allows only radial displacements and in turn this permits a one-dimensional description of the problem. The corresponding stresses are a radial and two equal hoop stresses.

The one-dimensional problem was analysed using 70 elements, with a single stress sampling location at the centre of each element. The problem has no intrinsic measure of scale and so, for convenience, the original cavity radius was set equal to unity. The outer boundary was set as a zero displacement node at a distance of 250, chosen to avoid artifacts of boundary conditions.

To capture the rapid variation of stress close to the CPT, the element spacing was set to logarithmically increase with distance from the cavity. Similarly, a second-order numerical difference was used to extrapolate the element stresses to the cavity wall to accurately capture the high stress gradients present at low strains.

Verification of finite element formulation

In addition to verifying the viscoplastic integration of NorSand, we also verified the finite element implementation of large-strain spherical-cavity expansion.

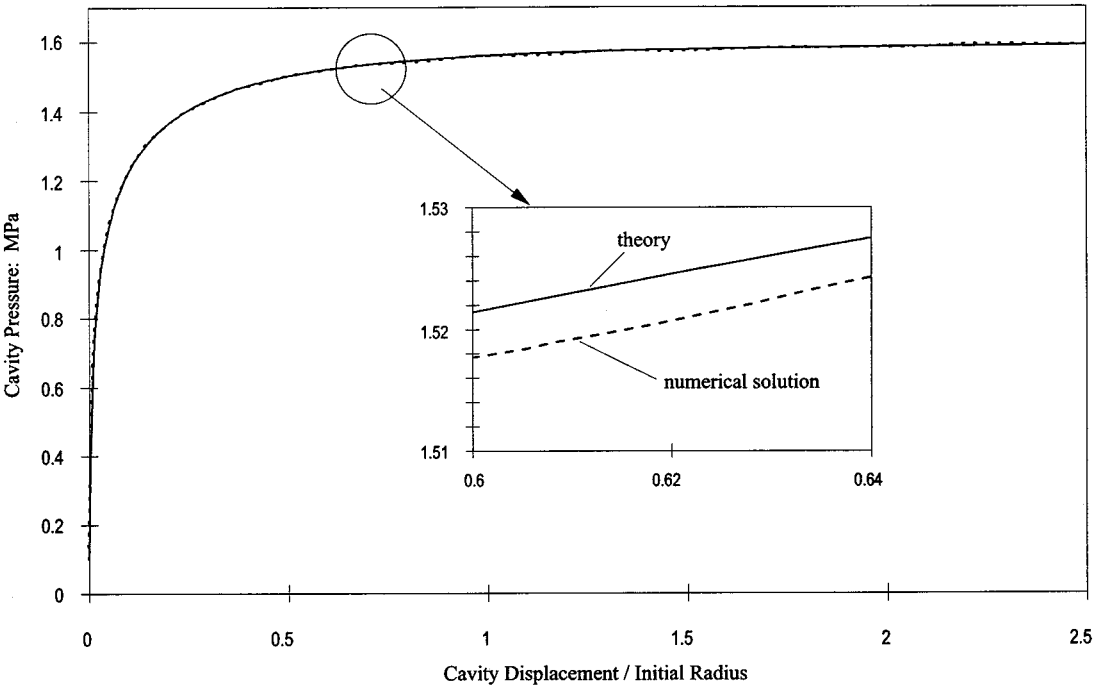

Figure 11. Comparison of theoretical and computed spherical expansion in Tresca material

The derivation of expansion for a spherical cavity in a Tresca material is standard[11,31,32] and leads to the following form between cavity pressure, P, and cavity radius, x:

$$P = \sigma_{h0} + \frac{4}{3} s_u + \frac{4}{3} s_u \ln\left[\frac{(x^3 - x_0^3)}{x^3} \frac{1}{1/(1 - e^{-1/I_r})}\right]^{1/3} \tag{27}$$

where σ_{h0} is the far-field geostatic stress, x_0 the initial cavity radius, s_u the undrained shear strength of the material, and I_r the rigidity index, G/s_u.

Comparison of the computed and theoretical spherical Tresca load–displacement relationship is presented in Figure 11 for an *in situ* horizontal stress of 0·1 MPa, an undrained shear strength of 0·2 MPa, and a rigidity index of 100. The initial cavity radius was unity. Figure 11 shows excellent agreement between the numerical formulation and the closed-form solution (27) throughout the entire loading curve.

Our second verification test compares the limit pressure from the numerical formulation with the analytical solution for a Mohr–Coulomb material. The solutions derived by Carter *et al.*[11] were used as they account for compression in the plastic region due to Poisson's ratio values less than 0·5, as well as allowing for net dilation.

The Mohr–Coulomb analysis again assumed a geostatic stress of 0.1 MPa, and an initial cavity radius of unity. The load–displacement curves for the spherical cavity in a cohesionless Mohr–Coulomb material with a friction angle of 30° and zero dilation, for Poisson's ratios of 0·1,

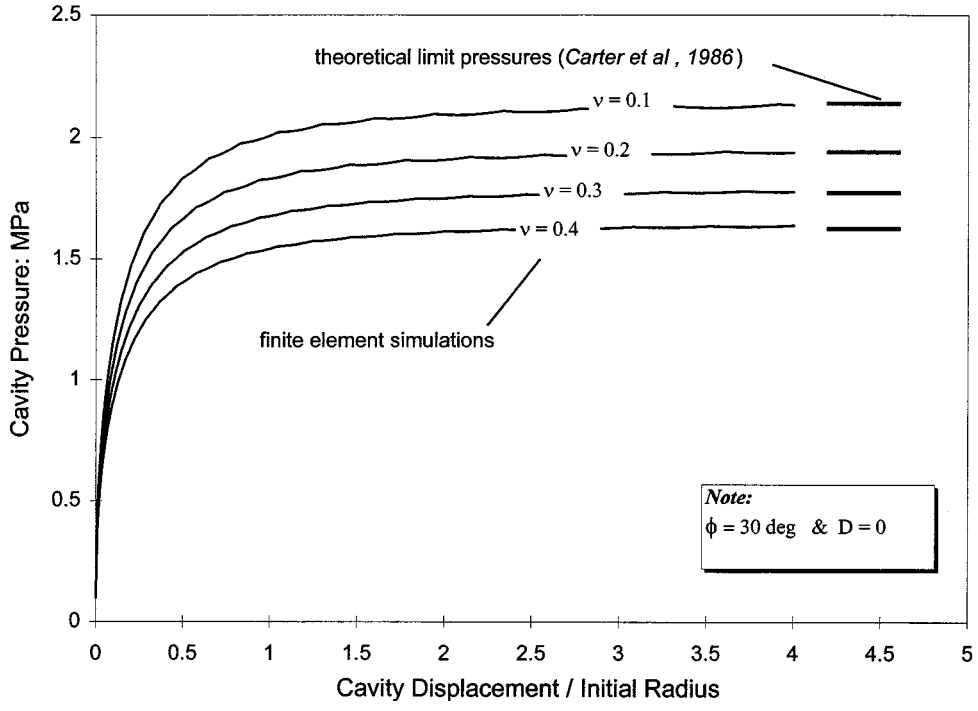

Figure 12. Theoretical and computed limit loads for Mohr–Coulomb material

0·2, 0·3 and 0·4, together with the corresponding limit loads, are given in Figure 12. All four numerical simulations agree with the theoretical solution to within 1 per cent. These simulations use the same mesh geometry, convergence tolerance, and displacement increment subsequently used for the NorSand simulations.

NUMERICAL RESULTS

Sand behaviour computed

The reason to use a 'good' sand model to analyse cavity expansion is that, in general, part of the domain will be critical, other parts strongly dilating, and other parts contractive with the exact behaviour being a function of position. Accordingly, it is helpful to look at the computed behaviour of the sand before examining the computed limiting pressures as a function of initial state.

The computed soil response obviously depends on the initial state of sand. However, to observe the key aspects of this behaviour, cavity expansion from a dense initial state may be considered. And, because computation starts from "at rest" conditions, the behaviour of an element close to the cavity wall provides sufficient information because there is no intrinsic scale in the analysis.

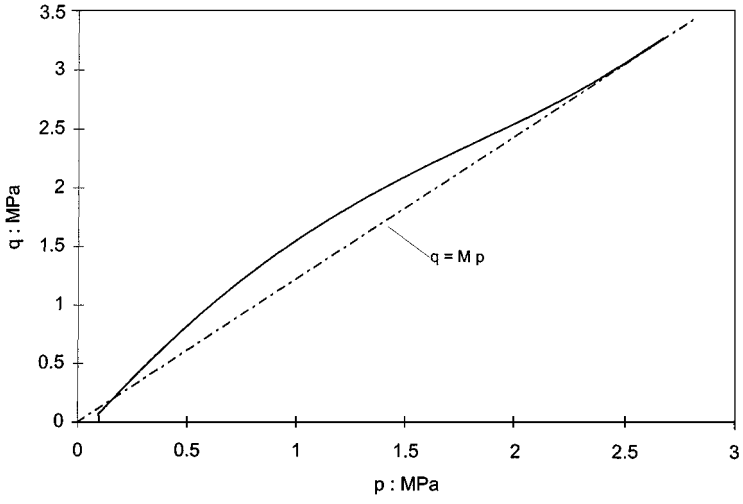

Figure 13. Computed stress path during cavity expansion

The stress path experienced as load is applied to the cavity wall is shown on Figure 13. As can be seen, the stress path is a long way from that of a triaxial compression test even though spherical cavity expansion is often referred to as being triaxial conditions. The stress path really amounts to a rapid excursion from isotropic conditions to the Mohr–Coulomb envelope followed by dilation up the envelope (which is curved because it is a function of the state parameter which decreases as the sand dilates to critical conditions). The corresponding stress–strain curve is shown on Figure 14 illustrating that a shear strain of more than 50 per cent is required to take the sand to its critical state.

In Figure 15 the state path of the sand is illustrated. Note how the sand moves up the CSL once that locus is attained. The reason for this is that the cavity has not reached its limiting expansion pressure at the time this particular element achieves critically, and so the element tracks up the CSL as the confining stress increases.

The pattern of state paths for different initial conditions is shown on Figure 16. All paths lead to the CSL. The behaviour is similar to that computed by Collins *et al.*[5] who used a different critical state model.

Comparison with CC data: Ticino Sand

Sixty-eight CC tests were carried out on normally consolidated Ticino sand by the Torino group, covering initial void ratios in the range $0{\cdot}5 < e < 0{\cdot}9$ and initial mean stress in the range $50\,\text{kPa} < p_0 < 500\,\text{kPa}$. For each of these tests a CPT resistance was measured. The CPT resistance was corrected for the experimental limitations of finite chamber size, a correction which varied from negligible for the looser tests to small for the dense ones (see References 2 and 8 for details of the correction procedure). These data have been summarised on Figure 17 as a plot of the dimensionless variable Q against the ψ_0 calculated from the CSL parameters for Ticino sand, where Q is the usual variable used in CPT work and is defined as

$$Q = (q_t - p_0)/p_0 \tag{28}$$

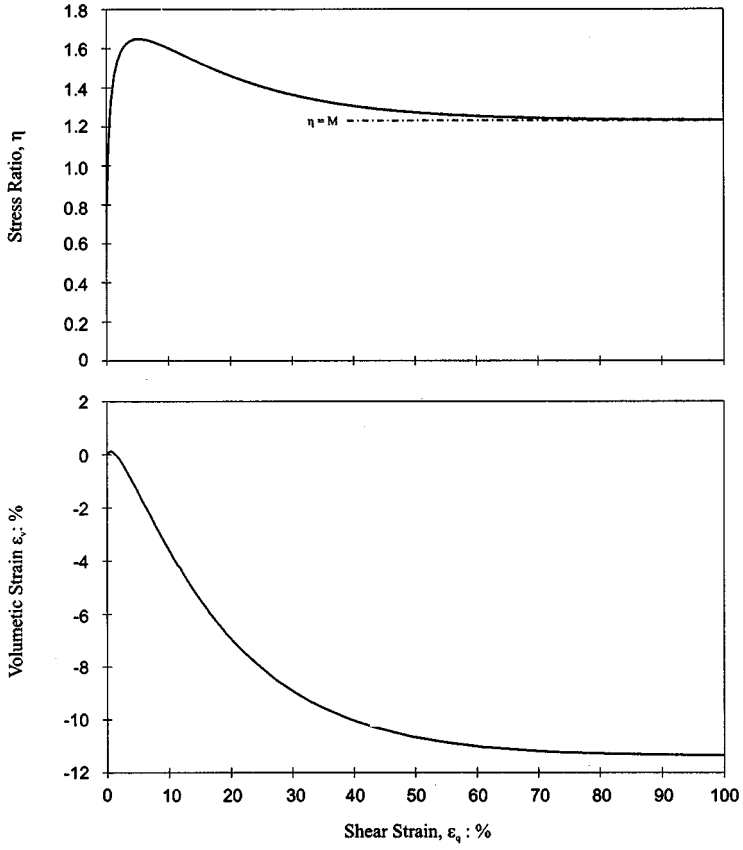

Figure 14. Stress-strain behaviour during cavity expansion

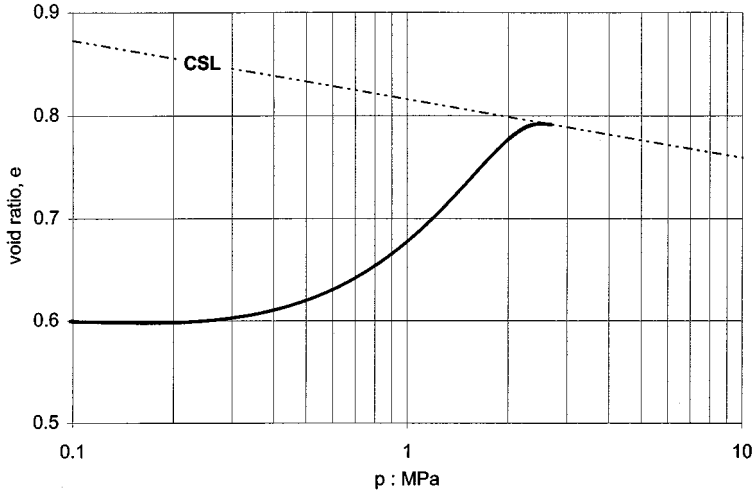

Figure 15. Computed state path during cavity expansion

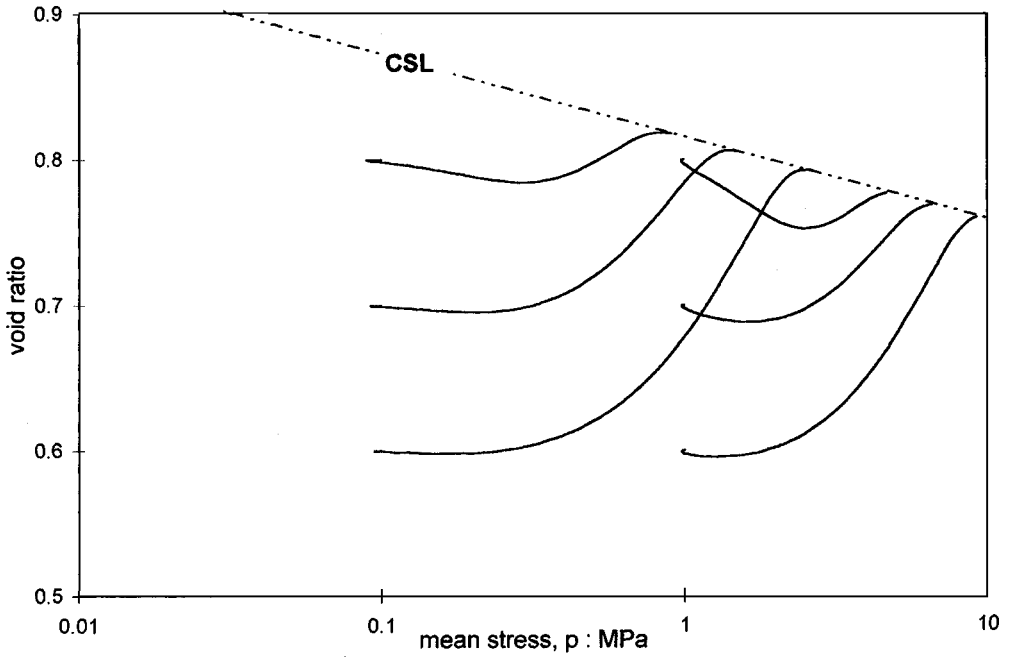

Figure 16. General pattern of state paths during cavity expansion

The numerical work took the e_0, p_0 pairs from the Ticino test program and a limiting cavity pressure, q_t, was computed for each pair using the material properties given on Table I. The numerical results are also presented on Figure 17, with the cross-comparison of computed against CC data on Figure 18. Looking at Figures 17 and 18, it can be seen that the numerical results give the same trends as the CPT in CC testing, but there is by no means an equivalence of the CPT to a spherical cavity expansion.

Use of equation (1) with constant k, m to recover ψ_0 from CC data causes bias, the error in estimated ψ_0 being plotted against stress level in Figure 19. A pattern of behaviour is seen that is consistent with the stress level effect noted by Collins *et al.*[5] and Sladen.[10] Although the bias is not as extreme as suggested by Sladen, the bias is important and ranges from too dilatant by $\Delta\psi_0 = -0{\cdot}02$ at $p_0 = 30\,\text{kPa}$ to insufficiently dilatant by $\Delta\psi_0 = +0{\cdot}08$ at $p_0 = 400\,\text{kPa}$: a bias across the stress range of engineering interest fully 25 per cent of the range of the parameter sought.

Equation (1) is dimensionless but does not explicitly include G even though G appears on the list of constitutive parameters. To clarify the situation, a series of finite element simulations were made with G given prescribed values rather than being related to the initial void ratio. The computed results for nine simulations are shown on Figure 20.

In Figure 20, the three simulations with $p_0 = 100\,\text{kPa}$ and $G = 64\,\text{MPa}$ lie on a line given by equation (1) to a high level of precision. Equally, keeping all else the same but changing the initial stress to $p_0 = 1000\,\text{kPa}$ gives three points on a different (but near-parallel) trend line: an apparent stress level effect. However, recognising that G needs to be brought into dimensionless form

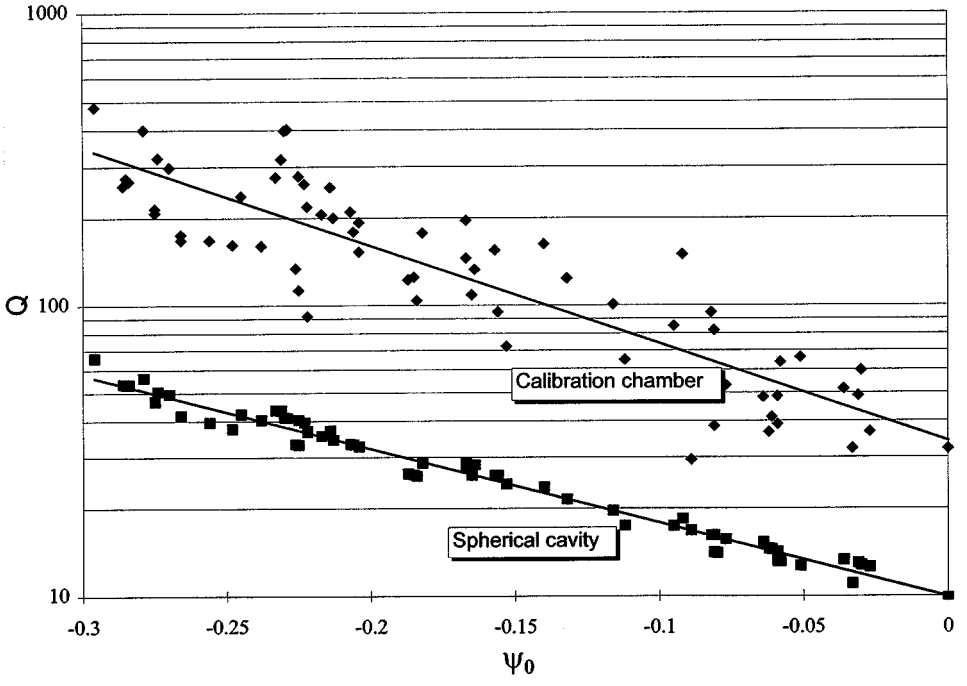

Figure 17. Q versus ψ_0 for Ticino sand

suggests that the grouping G/p_0 should be constant on any trend line, implying that $G = 640\,\text{kPa}$ at $p_0 = 1000\,\text{kPa}$ should recover the prior trend. The results of three additional simulations for this much stiffer G are also shown on Figure 20 and verify that indeed a single trend line is recovered. The scatter in the data around equation (1) is because a dimensionless parameter group has been omitted, not stress level per se.

The trend in Figure 20 can be fitted using equation (1) provided k, m are regarded as functions of the dimensionless group G/p_0 (amongst other constitutive parameters). For the material properties of Ticino sand a mapping is found (Figure 21):

$$k = 0{\cdot}75 + 1{\cdot}60\ln(G/p_0), \qquad m = 1{\cdot}30 + 0{\cdot}62\ln(G/p_0) \tag{29a, b}$$

Combining (29a, b) with (1) gives an equation for predicting the spherical cavity expansion pressure in Ticino sand:

$$Q = (0{\cdot}75 + 1{\cdot}60\ln(G/p_0))\exp(-(1{\cdot}30 + 0{\cdot}62\ln(G/p_0))\psi_0) \tag{30}$$

As a check, equation (30) is compared with the results given by Collins *et al.*[5] for Ticino sand in Figure 22. Both Collins *et al.* and ourselves analyse the spherical cavity, and both sets of analyses are based on the state parameter approach. However, the constitutive models are different, Collins *et al.* using a non-associated model and Mohr–Coulomb type yield surfaces with a purely elastic zone in the far field. In contrast NorSand has no elastic–plastic transition (for normally consolidated sands considered here) and both aspects of behaviour are present throughout the domain. There is a simple linear mapping between the two solutions which is apparently a direct

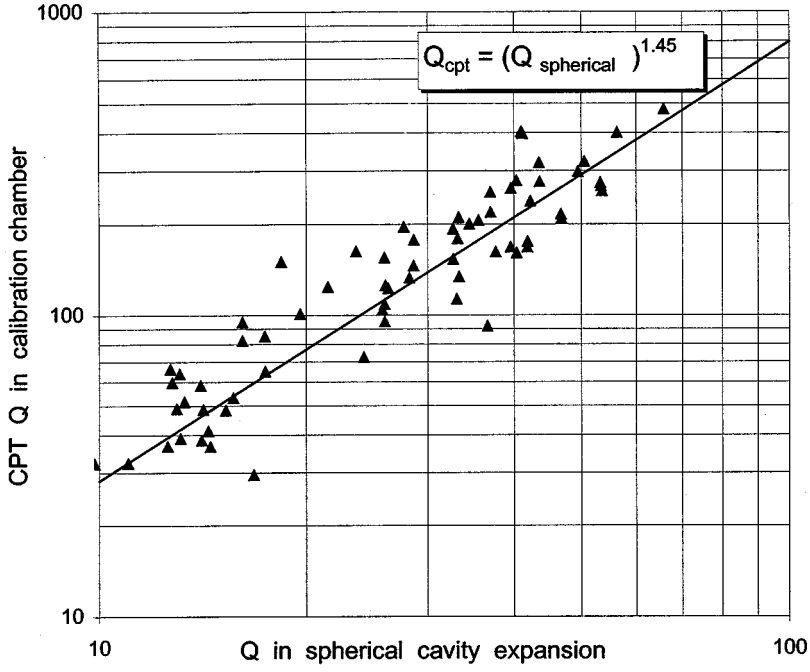

Figure 18. CPT in calibration chamber *versus* spherical cavity expansion: Ticino sand

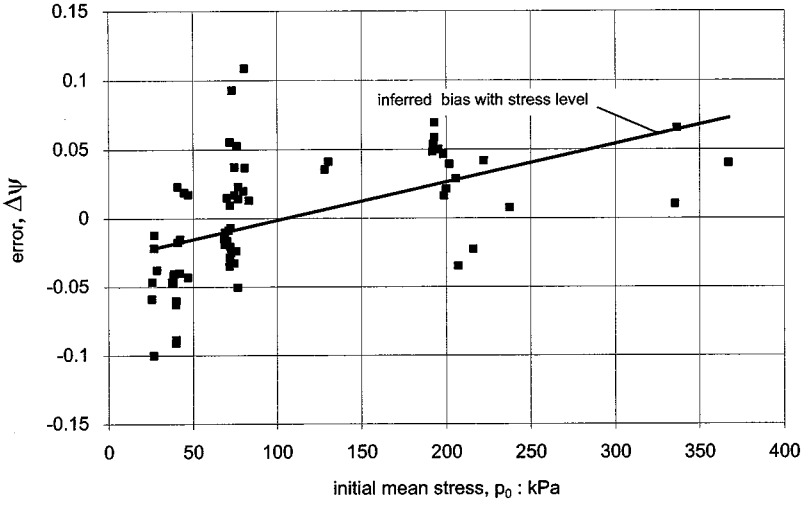

Figure 19. Bias in ψ_0 recovered from calibration chamber data using equation (1)

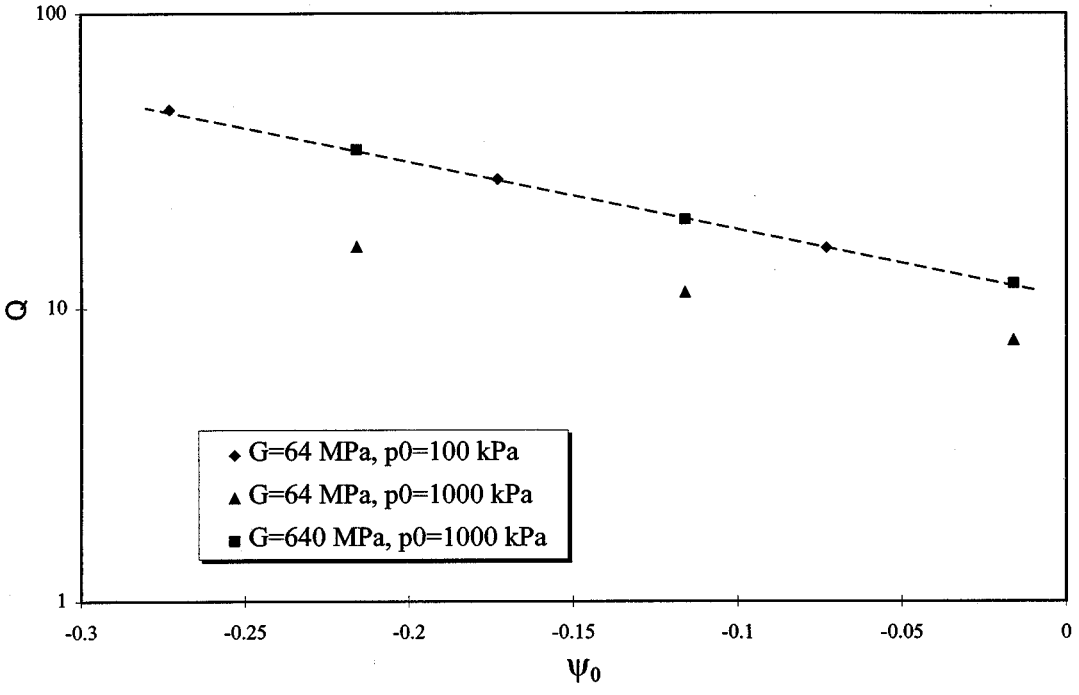

Figure 20. Effect of stress level on cavity expansion in Ticino sand

consequence of the differing constitutive idealizations and emphasizes the sensitivity of cavity expansion to volumetric strain (some further aspects of this are discussed later).

Comparison with CC data: Hilton Mine sand

As noted at the beginning, Hilton Mine sand was also chosen for simulation because its response to the CPT is far stronger than would be expected based on its relatively compressible nature. Twenty CC tests on Hilton Mine sand were reported by Harman[33] on normally consolidated Hilton Mine sand covering initial void ratios in the range $0{\cdot}65 < e < 0{\cdot}95$ and initial mean stress in the range $30\,\text{kPa} < p_0 < 200\,\text{kPa}$. For each of these tests, a CPT resistance was measured. The reported CPT resistances have been corrected for the experimental limitations of finite chamber size by Been *et al.*[2] and this corrected data is used here.

The numerical work took the e_0, p_0 pairs from the Hilton Mine test program and a limiting cavity pressure was computed for each pair using the properties for Hilton Mine sand given on Table I. Both the CC data and the corresponding numerical results (denoted by $H = 65$) are presented on Figure 23. Applying the spherical to CPT mapping established for Ticino sand to the Hilton Mine simulations gives a close match to the Hilton Mine CPT data at $\psi_0 = -0{\cdot}05$, although this match degrades for more dilatant states. The 40 per cent difference in CPT penetration resistance between Hilton Mine and Ticino sand is captured. The question then arises as to why the trend with denser states is not more closely modelled.

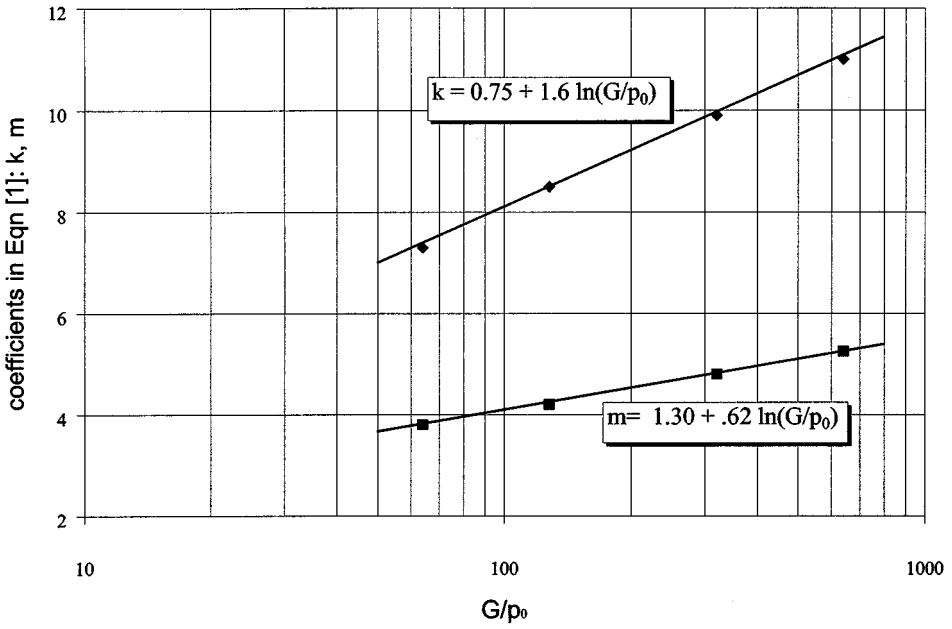

Figure 21. Effect of G/p_0 on spherical cavity expansion in Ticino sand

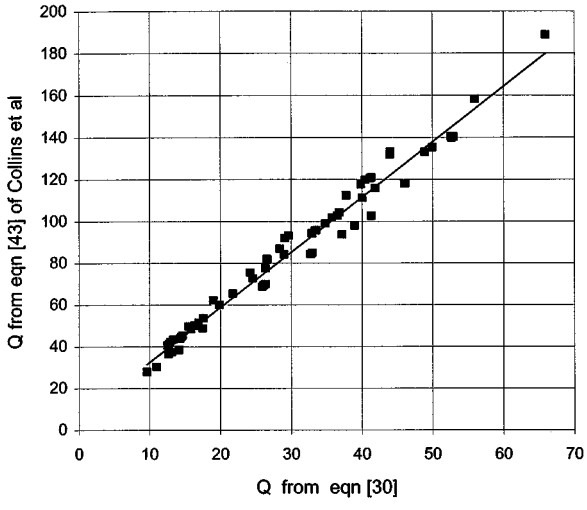

Figure 22. Comparison of solutions for spherical cavity expansion in Ticino sand

The trend of Q with ψ_0 is different with these two sands because in one instance (Ticino) the plastic hardening modulus H is treated as a function of ψ_0 while in the other it is a constant. Because the cavity limit pressure depends on plastic hardening, this necessarily produces different trends. Several uncertainties now need to be considered.

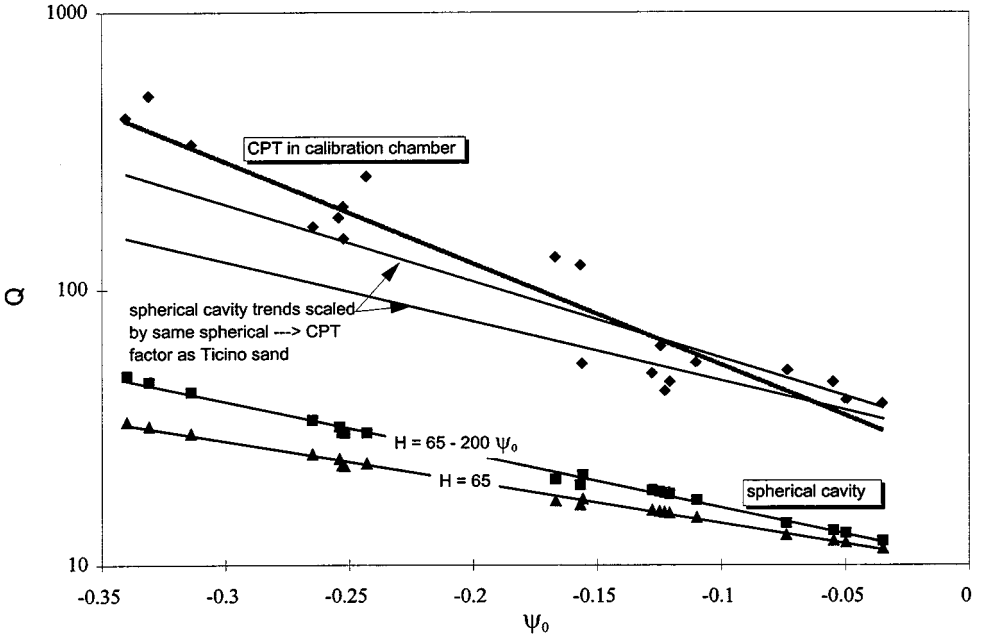

Figure 23. CPT in calibration chamber versus spherical cavity expansion, Hilton Mine sand

The Ticino CC data are so scattered that a range of trendlines can be drawn through the data. So, one possibility is that the computed trends for spherical cavity expansion correctly represent the real difference between Ticino and Hilton Mine sand and an incorrect trend has been inferred for the Ticino CC data.

Conversely, one may question the determination of H from triaxial tests on two counts. First, different stress–strain behaviours occur in sand for constant sand state depending on grain arrangement (what is often called fabric). Determining H from samples reconstituted in a different laboratory and using different procedures from the CC sand placement introduces in itself an uncertainty. Second, relatively few triaxial tests were carried out and these have significant scatter in the best-fit parameter sets so it is also uncertain that H, and any trends in H with state or stress level, have been completely identified. And of course we computed with assumed elastic properties for Hilton Mine sand since none were measured.

Thus, it is unwise to push the comparison of Hilton Mine with Ticino too far. Broadly, the correct relative penetration resistance is computed. Improvements can be obtained by quite modest pushing of the uncertainty bounds, as is also illustrated in Figure 23 where the trend for a sand with all the properties of Hilton Mine is illustrated with the sole exception that the hardening has been increased slightly to $H = 65–200\psi_0$ (this hardening rule keeps the relative softness of Hilton Mine to Ticino at all states and is not inconsistent with the limited triaxial test data available). With this modified view of Hilton Mine sand, we get a relationship between Hilton Mine and Ticino that shows a similar trend in spherical-cavity expansion as apparently exists in the CC results.

INVERSE FORM FOR INTERPRETATION OF CPT

Ticino sand

Although it is interesting to compute a CPT resistance, the purpose of the work is to estimate the *in situ* state from the CPT measurements. This requires an inversion of the relationships developed from the numerical simulations. Equation (30) is invertable to allow recovery of ψ_0 from spherical cavity expansion in Ticino sand:

$$\psi_0 = -\ln(Q/(0{\cdot}75 + 1{\cdot}60\ln(G/p_0)))/(1{\cdot}30 + 0{\cdot}62\ln(G/p_0)) \tag{31}$$

The performance of (31) against the numerical results is shown on Figure 24. There is an excellent correspondence between recovered ψ_0 and that specified as the initial conditions for the simulations. In terms of uncertainty in ψ_0, the error in using equation (31) is that ψ_0 can be recovered to a precision of better than $\Delta\psi_0 = \pm 0{\cdot}004$ at a 90 per cent confidence level and without bias (Figure 25). In the case of the spherical cavity, including the dimensionless stiffness G/p_0 in the inversion recovers ψ_0 well within the target for a useful method and corresponds to an unbiased accuracy of about 1 per cent in the parameter sought. Clearly this represents a goal for real CPT interpretation and shows that in principle the interpretation of CPT data can offer the same precision as the CPT repeatability.

Imperfect recovery of the initial state arises because the exponential form of (1) is a close but not perfect fit to the results; this can seen on Figure 20 where the $G/p_0 = 640$ results show a slight

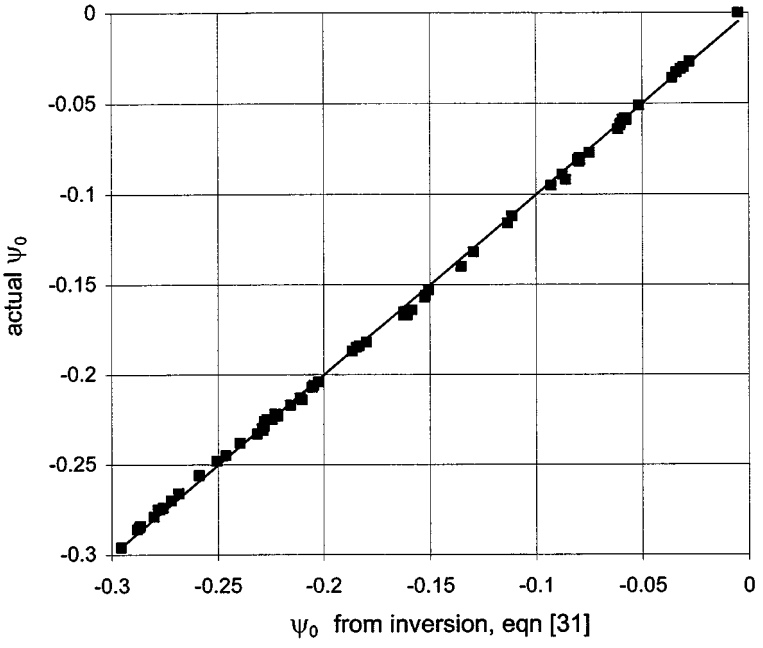

Figure 24. Recovery of ψ_0 from numerical simulations in Ticino sand

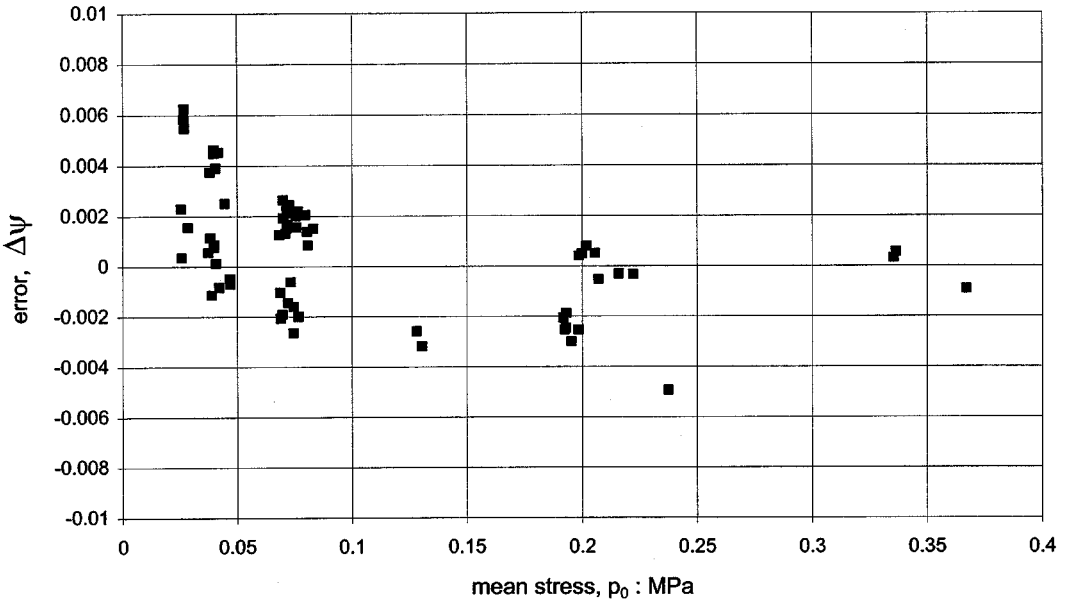

Figure 25. Bias in ψ_0 recovered from numerical simulations in Ticino sand

curvature around the exponential trend line. Considerable care is required in fitting analytic functions to the numerical trends to preserve precision through the subsequent inversion.

Turning to the CPT in CC testing, from Figure 18 the relationship between the CPT resistance Q_{cpt} and the spherical cavity limit pressure Q_{sph} is (for Ticino sand)

$$Q_{cpt} = (Q_{sph})^{1\cdot45} \tag{32}$$

Substituting (32) in (31) gives an inverted form for recovery of ψ_0 from CPT data in Ticino sand:

$$\psi_0 = -\ln(Q_{cpt}^{0\cdot69}/(0\cdot75 + 1\cdot60\ln(G/p_0)))/(1\cdot30 + 0\cdot62\ln(G/p_0)) \tag{33}$$

Equation (33) recovers ψ_0 from the CC data in Ticino sand to a precision of $\Delta\psi_0 = \pm 0\cdot07$ at a 90 per cent confidence level as shown on Figure 26. The recovered ψ_0 is sensibly unbiased with regard to mean stress level, Figure 27. Comparing Figure 27 with Figure 19 (which uses the original Been *et al.* formulation), one sees that the removal of bias is accompanied by a small improvement in the uncertainty but that the scatter remains large.

The magnitude of the uncertainty in recovering the initial CC void ratio from the CPT data may be surprising, but is bound up with the CC data itself. For example, in the case of the Ticino CC work, tests E139 and I169 have virtually identical initial conditions in terms of stress state, geostatic stress ratio (K_0), and void ratio. Yet the recorded CPT resistance differs by more than a factor of 2. Clearly no valid interpretation can recover two different values when all else is equal, and correspondingly this introduces an apparent uncertainty. It is an apparent uncertainty because these tests contain an unmeasured variable, G, which can easily vary by $\pm$ 50 per cent because of sample preparation all else equal. A factor of $\pm$ 50 per cent on G will produce about $\pm 0\cdot03$ on ψ_0, which is about half the residual uncertainty.

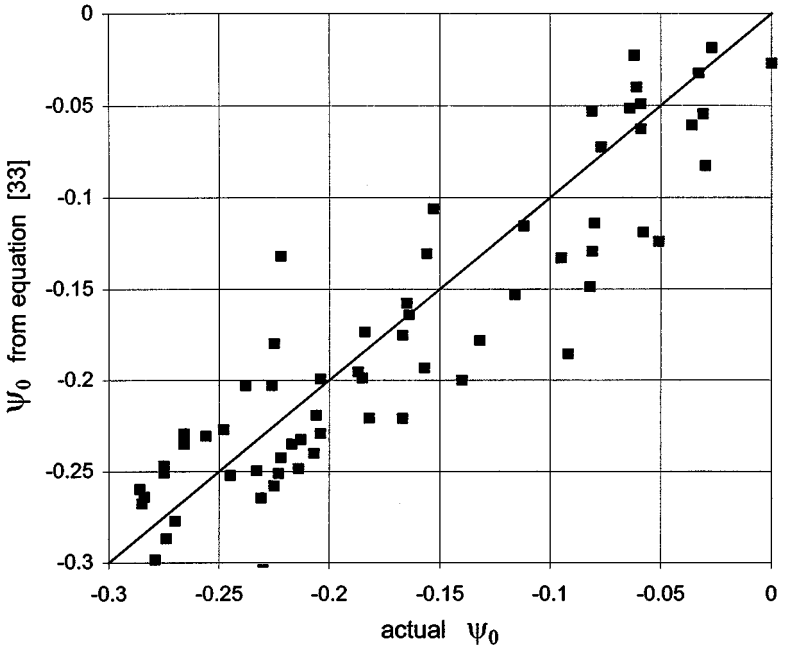

Figure 26. Recovery of ψ_0 from Ticino calibration chamber data

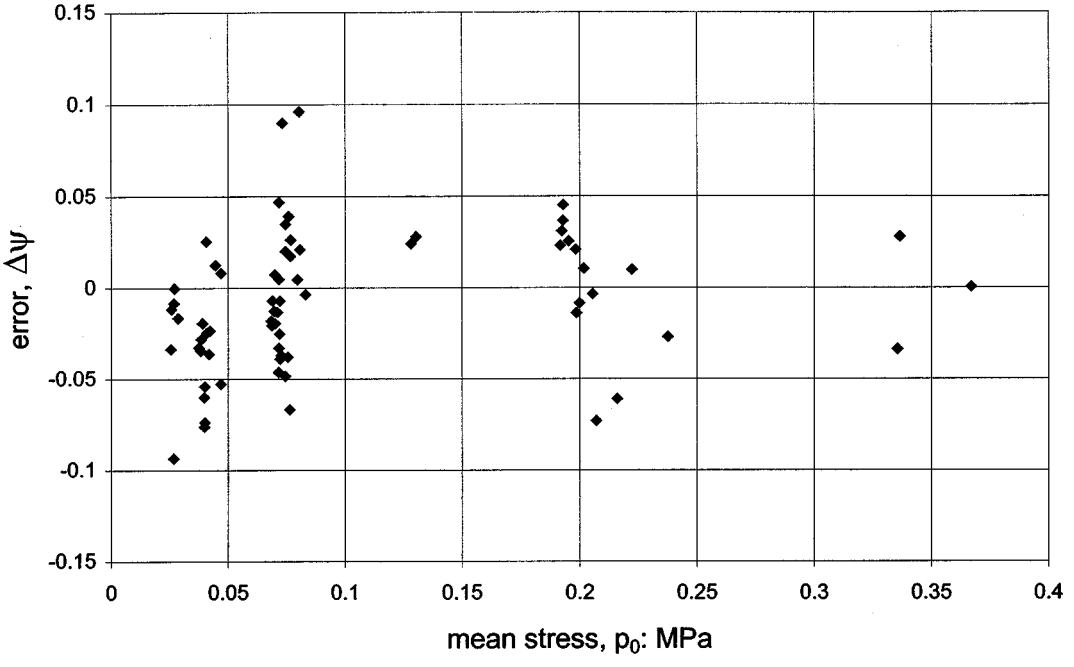

Figure 27. Bias in recovered ψ_0 for Ticino calibration chamber data

General inverse form

We noted at the outset of this paper that while the so-called stress level issue had attracted attention, a far weaker aspect of Been *et al.*[2] was the speculative reliance on λ to scale the Q–ψ_0 relationship for sands. We have already shown the influence of G as an additional variable, but a brief look back at Table I will illustrate that there are a further four parameters (M, N, H, v) all of which could affect the relationship between Q and ψ_0. These parameters must be recognized in an inverse form of relationship for general CPT interpretation in sand. The importance of these material properties was investigated by varying each in turn about a central case, as illustrated on Figures 28–32 inclusive and summarized on Table II. The ranges selected for analysis represent those encountered with sands to silty sands and thus the relative effects indicate the relative importance of each parameter to the available precision in inferring sand state from CPT data.

Given the results of the sensitivity study, Figures 28–32, and the previously determined effect of dimensionless elastic shear stiffness (equation (29)), a first estimate of the form of a universal inverse interpretation function can be developed by assuming that each of the parameters independently affect the two coefficients k, m in the relationship of Q with ψ_0 and approximating the trends in the numerical data with analytic expressions. This leads to the following expressions:

$$k = f_1(G/p_0)\, f_2(M)\, f_3(N)\, f_4(H)\, f_5(\lambda)\, f_6(v) \tag{34a}$$

$$m = f_7(G/p_0)\, f_8(M)\, f_9(N)\, f_{10}(H)\, f_{11}(\lambda)\, f_{12}(v) \tag{34b}$$

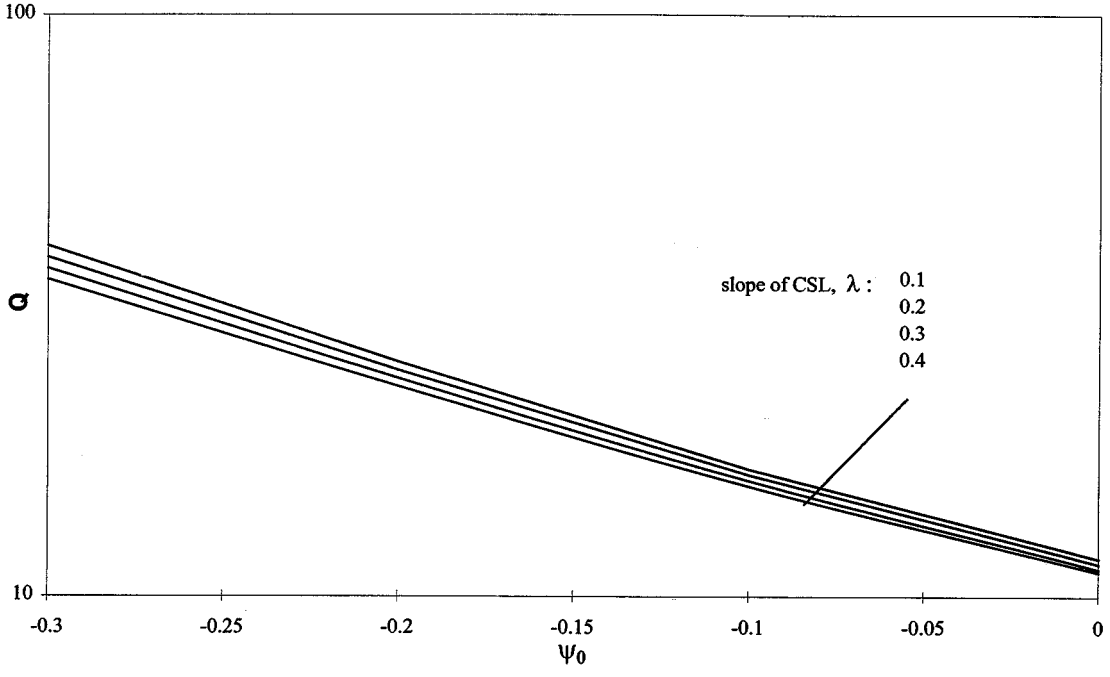

Figure 28. Influence of λ on expansion pressure

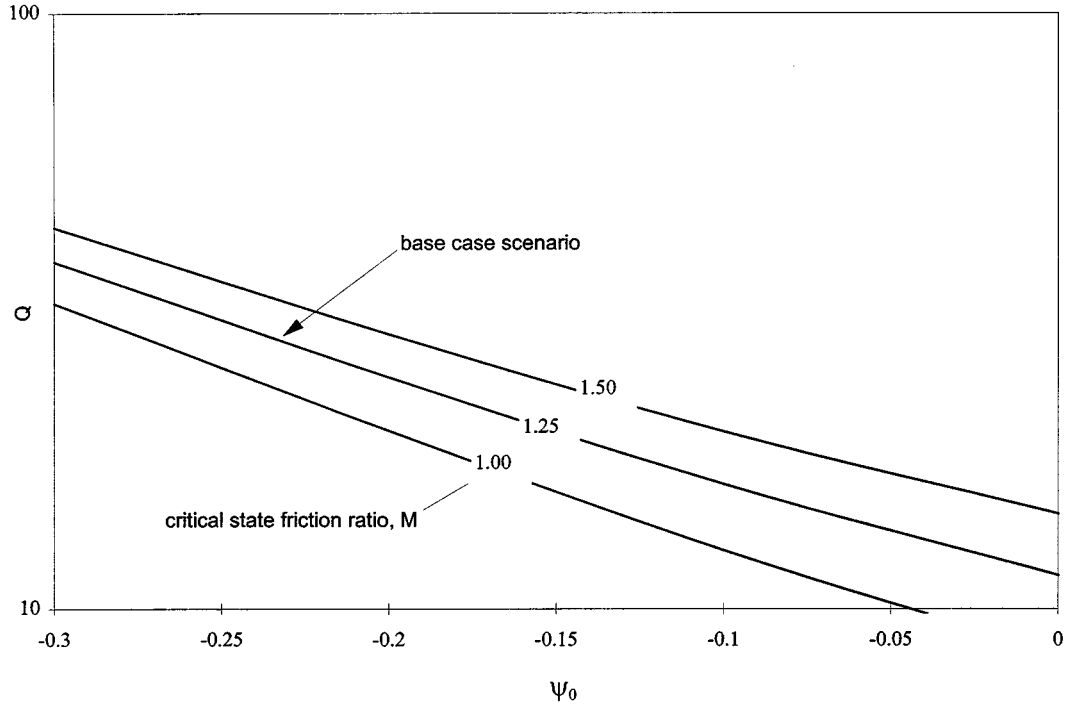

Figure 29. Influence of M on expansion pressure

where the fitted functions f_1–f_{12} are given on Table III. The first estimate of the general framework for interpreting spherical-cavity expansion then comprises these 12 equations, which give the coefficients k, m through (34) since all the independent variables in f_1–f_{12} are known, and which are then used in the inverse form of (1):

$$\Psi_0 = \frac{\ln(Q/k)}{m} \tag{35}$$

Note that f_4 and f_{10} have been determined for constant H. If, like Ticino sand, H depends on ψ_0 then these two equations can still be used to determine m allowing for this dependency.

The adequacy of this approximation to a general inverse form was investigated by assigning uniform distributions to the various parameter and initial state ranges, and then randomly selecting ten realizations and computing the cavity pressures. In turn, these cavity pressures were input to the approximate general inverse form to compute the inferred initial state. Figure 33 compares the true (specified) initial state and that inferred through application of the approximate inverse form. Table IV gives the parameter combinations realized to represent these 10 arbitrary sands.

As can be seen from Figure 33, the recovered ψ_0 falls within $\pm$ 0·01 of the true value for nine cases and only slightly outside this uncertainty band in the tenth. The suggested approximation to a general inverse form for the CPT interpretation comes close to the precision goal identified as

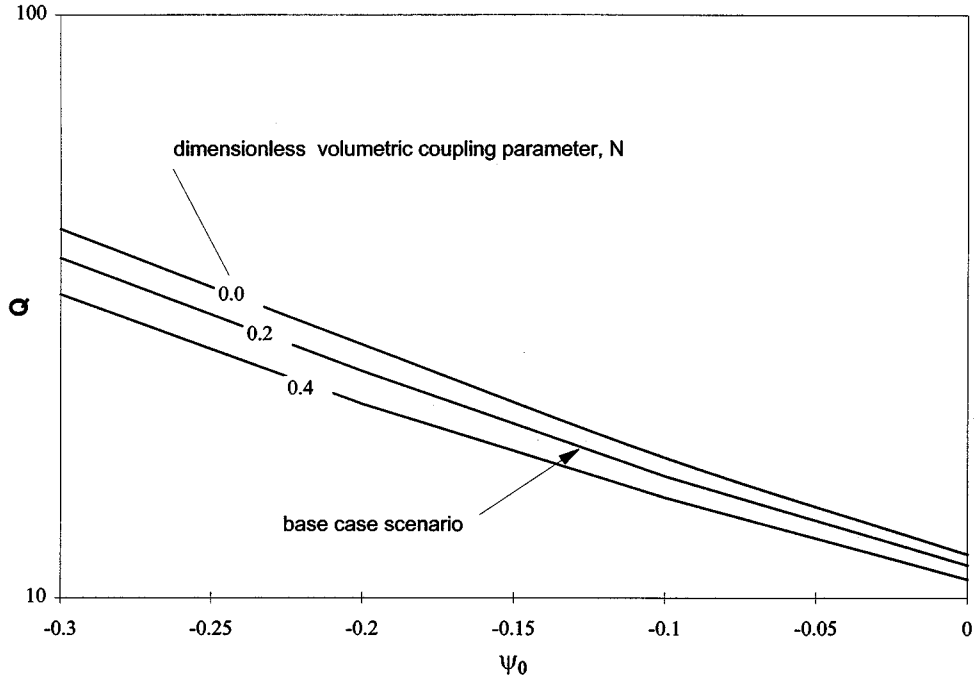

Figure 30. Influence of N on expansion pressure

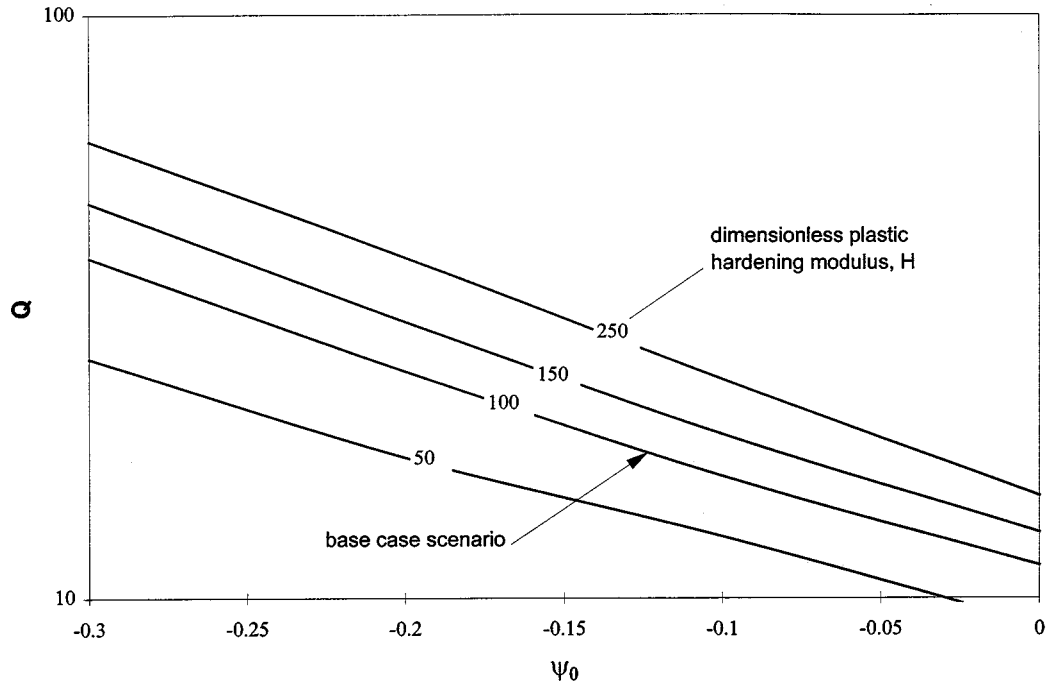

Figure 31. Influence of H on expansion pressure

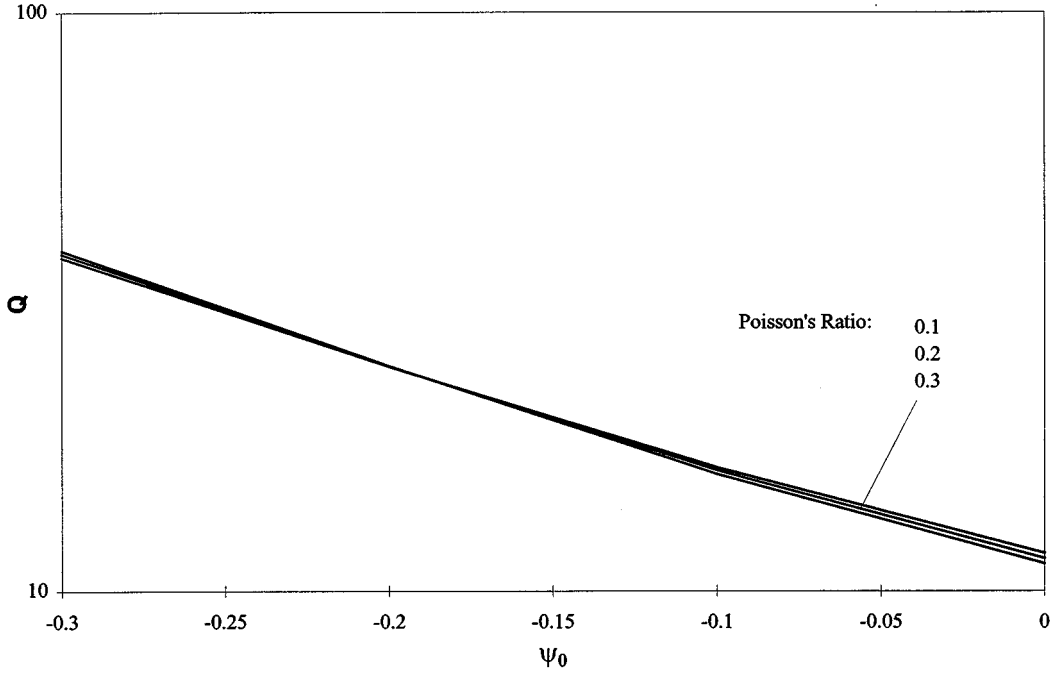

Figure 32. Influence of Poission's ratio on expansion pressure

Table II. Parameter variation in sensitivity analysis

Parameter	Base case	Variation	Effect on q
λ	0·02	0·01–0·04	Small
M	1·25	1·0–1·50	± 25%
N	0·2	0·00–0·40	± 15%
H	100	50–350	± 25%
v	0·2	0·1–0·3	Negligible

desirable at the beginning of this paper. Importantly, the approximate inverse form is sufficiently simple to be readily applied in CPT data processing software. Recall, however, that here we are dealing with spherical cavity expansion and there is an additional uncertainty unresolved in the present work regarding the consistency of the mapping between spherical cavity expansion and CPT penetration in a sensibly infinite medium.

DISCUSSION

Although we have commented on issues as they have arisen through the paper, there are four issues which require further discussion: the role of G and its independence; other constitutive

Table III. Approximate expressions for general inverse form

Function	Approximation
$f_1(G/p_0)$	$3{\cdot}79 + 1{\cdot}12\ln(G/p_0)$
$f_2(M)$	$1 + 1{\cdot}06\ (M - 1{\cdot}25)$
$f_3(N)$	$1 - 0{\cdot}30\ (N - 0{\cdot}2)$
$f_4(H)$	$(H/100)^{0.326}$
$f_5(\lambda)$	$1 - 1{\cdot}55\ (\lambda - 0{\cdot}01)$
$f_6(v)$	Unity
$f_7(G/p_0)$	$1{\cdot}04 + 0{\cdot}46\ln(G/p_0)$
$f_8(M)$	$1 - 0{\cdot}40\ (M - 1{\cdot}25)$
$f_9(N)$	$1 - 0{\cdot}30\ (N - 0{\cdot}2)$
$f_{10}(H)$	$(H/100)^{0.15}$
$f_{11}(\lambda)$	$1 - 2{\cdot}21\ (\lambda - 0{\cdot}01)$
$f_{12}(v)$	Unity

Table IV. Randomly realized parameter combinations to test general inversion

Realization	M	N	H	G/p_0	v	p_0(kPa)	ψ_0	Γ	λ
1	1·11	0·18	63	749	0·24	392	− 0·294	1·08	0·014
2	1·26	0·07	167	917	0·22	379	− 0·006	0·87	0·027
3	1·18	0·23	176	496	0·18	42	− 0·173	0·96	0·024
4	1·34	0·30	163	789	0·19	323	− 0·163	0·94	0·014
5	1·32	0·23	114	785	0·16	380	− 0·115	0·90	0·014
6	1·20	0·08	194	229	0·34	183	− 0·209	1·03	0·023
7	1·37	0·38	286	515	0·20	190	− 0·017	0·89	0·033
8	1·29	0·16	289	710	0·27	328	− 0·172	0·96	0·016
9	1·12	0·34	84	686	0·33	40	− 0·086	0·89	0·028
10	1·24	0·33	55	609	0·27	197	− 0·034	0·82	0·017

parameters; alternative constitutive idealizations; and, the adequacy of the spherical cavity analogy for the CPT.

The influence of G on the CPT is well known in the CPT literature but it appears that—to date—the underlying idea has been that the CPT responds to void ratio (or relative density) and that the relationship to G then follows through the dependence of G on void ratio (e.g. as in (10) above). The present analyses show this view to be false. Although G may have some dependence on void ratio, there is sufficient uncertainty in that relationship and sufficient variability because of other factors such as particle arrangement, that G must be treated as an independent variable. And, G must be accounted for in any dimensionless framework. Using a dependent relationship like equation (10) simply hides a term with the units of stress and this in turn leads to errors in attribution of bias. Given that G is sensibly independent then there is no alternative but to measure it directly.

It is unfortunate that the CC test programs carried out so far have not measured G during the tests as this body of work represents a large research effort over many years. Clearly, it is essential

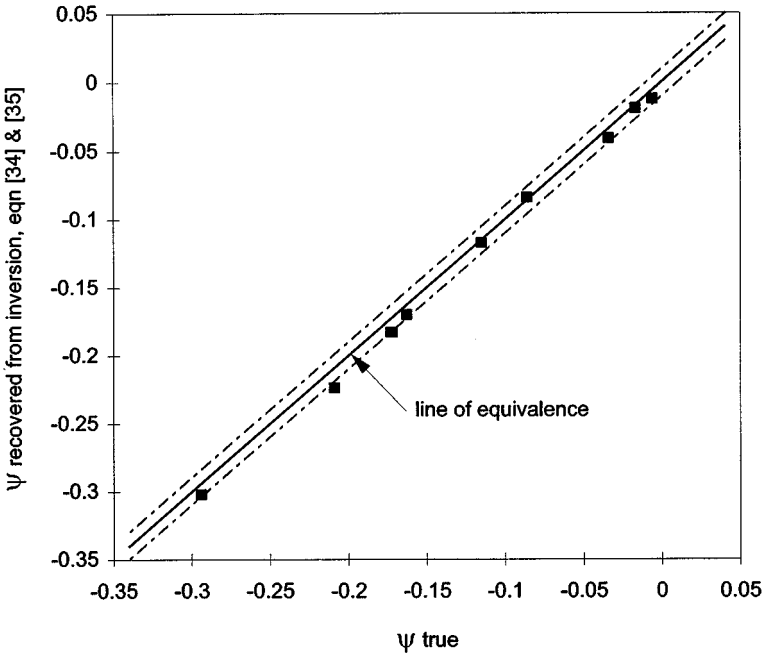

Figure 33. Performance of approximate general inversion on 10 sands with randomly chosen properties

that future CC programs include the measurement of G in every test, which is simply done these days with bender elements. Equally, G should be measured in every field situation in which the CPT data is to be interpreted quantitatively—this is not onerous, expensive, or difficult with modern seismic CPT equipment.

One of the clear results of the present work is how two parameters ignored in widely used frameworks of CPT interpretation (e.g. Reference 1), the critical stress ratio M and the dimensionless plastic hardening modulus H, dominate the different response of the CPT in different sands. It is unsurprising that engineering parameters presently inferred from CPT data are often regarded as uncertain. An interesting further question then occurs: What else might have been missed? Two factors are immediately apparent.

We have used the conventional semi-log approximation for the CSL. However, it is becoming apparent (e.g. the data presented by Reference 18) that this approximation becomes increasingly poor once the mean stress exceeds about 2 MPa and this stress level may be exceeded adjacent to the CPT probe in many cases. One reason for the deviation from the semi-log approximation may be sand grain breakage. Clearly there is scope for including grain fracture strength/toughness in a general framework for the CPT.

The apparent curvature of the CSL in e–ln(p) space also raises an interesting issue regarding the minimum void ratio. As mean stress increases the sand cannot compress for ever. At some point a sintering or other like process will occur and the sand will cease to be particulate and become rock. Conceptually, the onset of such processes is characterized by the minimum void ratio and this suggests that the minimum void ratio might be a parameter in a complete framework for the

CPT given the high-stress levels often encountered in testing dense sands. The minimum void ratio may be important at lower stress levels because one of the reasons the present cavity pressure simulations have diverged from the CPT resistance is the elastic compression implicit in a power-law shear modulus when combined with a constant Poisson's ratio. If the elastic volumetric model was refined, say by inclusion of a minimum void ratio to progressively increase the elastic bulk modulus, then the divergence of the cavity solution from the real CPT should be reduced.

A further concern is the plastic hardening. It is unclear that the hardening encountered in reconstituted laboratory samples is similar to that of the same sand *in situ*. Which then raises some interesting ramifications for the CPT given the importance of H to a reasonably precise framework. Perhaps the way forward is to determine H *in situ*, possibly with a self-bored pressuremeter, but to date there is no reliable method for this.

Turning to alternative constitutive idealizations, the question arises: Are the conclusions reached here specific to the mathematical idealization used, or are they general? Although one might suggest that the parameters used are specific to NorSand, in reality related parameters will occur in any good constitutive model. M is simply an identity of the critical state friction angle and that is widely accepted. H is a plastic modulus and any work hardening model will have at least one such parameter (and many models have several). G and v will always occur because there is at least some elasticity, and in fact volumetric elasticity can be of the same order of importance as volumetric plasticity with sands. The volumetric compressibility under shear is governed by λ and it is difficult to deny its relevance since the extreme strain adjacent to the CPT takes the sand to the critical state and the sand adjacent to the CPT reaches the critical state before the limit pressure occurs.

What we see in the present work is that these parameters all contribute to the scaling of the Q–ψ_0 relationship. And because interpreting CPT data to infer *in situ* state is an inverse boundary value problem, minor approximations are amplified so that neglecting any of these parameters substantially degrades the accuracy of the estimated state. In the case of a single sand, the numerical approach can be used to develop a mapping similar to that proposed by Been *et al.*[8] although now explicitly including shear modulus, which will allow *in situ* state to be estimated as accurately as the CPT data itself provided that G and p_0 are both independently measured. In the more general case of approximating all parameter combinations with analytical expressions, the suggested approximation of a general inverse form recovers ψ_0 with slightly increased uncertainty but still within the precision required for a useful method.

A striking aspect of the CPT literature is the absence of a general framework of quantitative interpretation despite the effort invested in understanding this test over the years. Our present results show why it is so: there are far more parameters of first-order significance to a general inverse method than has been recognized to date. And, the interplay of these parameters is distinctly non-linear. Certainly, relatively few chamber tests empirically interpreted will not produce a method with general applicability. In turn, this implies numerical simulations must play a far stronger role in the CPT industry in the future.

Naturally, this leads to questions about the adequacy of the spherical cavity idealization. Spherical-cavity numerics, such as those used in this paper, lend themselves to automated calculation of Q–ψ_0 mappings which can be run quickly on pentium class PC's and so be widely useful. However, it is clear that spherical cavity expansion is not a CPT and for the spherical cavity to be used as the basis of a mapping method we need to know the relationship between the cavity solution and the CPT is at least systematic, and preferably unchanged from sand to sand.

The present work is unclear on this latter point because of uncertainties in the experimental data, and that from the calibration chamber work in particular. In the short term there is considerable merit in a systematic analysis of the CPT using real geometry, steel-sand friction, etc.

CONCLUSIONS

Determining sand state from CPT data has been considered from the viewpoint of spherical-cavity expansion using a constitutive model (NorSand) that closely matches the sand's behaviour. In particular, the suggested universal approach to CPT interpretation proposed by Been *et al.*[2] has been investigated.

This investigation has shown that the apparent stress level bias in the method of interpreting CPT data in sands proposed by Been *et al.* is actually caused by neglect of a dimensionless parameter group, G/p_0. A revised form of the interpretation equation is developed and shown to recover the initial state without bias and to a high precision in the case of the numerical simulations for Ticino sand.

On a practical front, it is vital that further calibration chamber programs include measurements of G in each and every test if unnecessary uncertainty is to be removed from this commercially important test method. Likewise, field work in which the CPT data will be used quantitatively must include routine measurements of the shear modulus profile.

We then extended the analysis to consider a general framework for interpretation of the CPT. There are five sand properties that affect the CPT response and which must be involved in a universal CPT interpretation framework. Fitting analytic expressions to the numerical results is approximate and leads to lesser accuracy in the inversion for interpretation of CPT data than available when a specific sand is analysed in detail but still allows ψ_0 to be recovered within uncertainty bounds for a useful method. Given the ease with which numerical simulations can be undertaken, this suggests a far stronger role for numerically-based CPT interpretation in the future. However, it is desirable to move beyond the spherical cavity and analyse soil penetration using the real CPT geometry because of unresolved uncertainties between spherical cavity limit pressure and CPT resistance.

Finally, thought needs to be given to the measurement of the plastic hardening modulus of sand *in situ* since it is both important to the interpretation of CPT data and itself dependent upon the deposition, age and other geological aspects of the deposit.

APPENDIX I. NOTATION

a	nodal displacement
B	elastic strain–displacement matrix
B_L	strain–displacement matrix for incremental component of finite strain
Dee	elastic axisymmetric stress–strain matrix
D	plastic strain rate ratio (dilatancy)
e	void ratio
G	elastic shear modulus
h_v	volumetric hardening modulus
h_q	shear hardening modulus
H	shear hardening coefficient
I_r	rigidity index, G/s_u

K_0 Cauchy strain stiffness matrix
K_L part of the displacement component of the finite strain stiffness matrix
K_T finite strain stiffness matrix
K_θ initial stress or geometric matrix
L element length
M stress matrix
M critical state coefficient, a material property
N volumetric coupling coefficient, a material property
p mean stress ($= (\sigma_r + 2.\sigma_\theta)/3$)
p_0 *in situ* mean stress
q deviator stress ($= \sigma_r - \sigma_\theta$)
q_t limiting cavity pressure, CPT penetration resistance
Q dimensionless cavity or CPT bearing capacity factor ($= (q_t - p_0)/p_0$)
r radius
s_u undrained shear strength of the material
u radial displacement
V volume
v specific volume ($= 1 +$ void ratio)
x_0 initial cavity radius
ε total finite strain
ε_L incremental component of large strain
ε_r radial finite strain
ε_S Cauchy 'small' strain
ε_v volumetric strain $= (\varepsilon_r + 2\varepsilon_q)$
ε_q shear strain ($= 2/3(\varepsilon_r - \varepsilon_\theta)$)
$\varepsilon_{\theta 1}$ circumferential finite strain
$\varepsilon_{\theta 2}$ circumferential finite strain
Γ location of mapping of critical state locus in e–ln(p) space as measured by $e_c|_{p=1}$
λ slope of CSL in e–ln(p) space
ν Poisson's ratio
η stress ratio ($= q/p$)
σ stress vector
σ_{h0} *in situ* horizontal stress
ψ state parameter

APPENDIX II: FLOW CHART FOR NUMERICAL FORMULATION

Read in material properties
Initialize original state
Define geometry & number of steps
Define elastic stress–strain matrix, *Dee*
Set initial element stresses
Loop number of steps
    Iterations = 0
    Null loads, excess loads (bodyloads), incremental strain $\Delta\varepsilon$, incremental plastic strain $\Delta\varepsilon_p$, stiffness matrix

Update nodal co-ordinates
Assemble displacement component of stiffness matrix, $K_0 + K_L$
Add convected term, K_θ, to stiffness matrix
Set stiffness matrix, K, to fix nodal displacement at cavity wall to incremental displacement
Invert K matrix
Loop Iterations
Fix displacement at cavity wall & outer boundary
Compute nodal displacements from $\{\delta\} = [K]^{-1}\{f\}$
Check whether convergence criterion is reached
Loop Elements
$d\varepsilon = B\,da$ total strain increment
$d\varepsilon_e = d\varepsilon - d\varepsilon_p$ elastic strain increment
$\Delta\sigma = Dee\Delta\varepsilon_e$ elastic stress increment
$\sigma = \sigma_{step-1} + \Delta\sigma$ 'new' stress
Compute new NorSand yield surface
Does element stress state exceed yield?
No
continue to next element
Yes
calculate $d\varepsilon_{vp}$, increment viscoplastic strain rate
$d\varepsilon_{vp} = d\dot{\varepsilon}_{vp}\,dt$ increment of viscoplastic strain this iteration
$\varepsilon_{vp} = \varepsilon_{vp\,iter-1} + d\varepsilon_{vp}$ track viscoplastic strain this increment
$\int B^T Dee\varepsilon_{vp}$ calculate bodyloads incremen
bodyloads = $\text{bodyloads}_{iter-1}$ + bodyloads increment
Next Element
Did any element yield this iteration?
Yes
Continue to next iteration
No
Recover element stresses and strains for all elements
Project stresses to cavity wall
Update element in each element
Output element stresses, strains, void ratio, etc.
Next displacement increment

REFERENCES

1. P. K. Robertson and R. G. Campanella, 'Interpretation of cone penetration tests. Part I: Sand', *Can. Geotech. J.*, **20,** 718–733 (1983).
2. K. Been, M. G. Jefferies, J. H. A. Crooks and L. Rothenberg, 'The cone penetration test in sands: Part II, general inference of state', *Geotechnique*, **37,** 285–299 (1987).
3. K. Been and M. G. Jefferies, 'A state parameter for sands', *Geotechnique*, **35,** 99–112 (1985).
4. M. D. Bolton, 'The strength and dilatancy of soils', *Geotechnique*, **36,** 65–78 (1986).
5. I. F. Collins, M. J. Pender and W. Yan, 'Cavity expansion in sands under drained loading conditions', *Int. J. Numer. Anal. Meth. Geomech.*, **16,** 3–23 (1992).
6. M. G. Jefferies, 'Nor-Sand: a simple critical state model for sand', *Geotechnique*, **43** (1), 91–103 (1993).

7. M. T. Manzari and Y. F. Dafalias, 'A critical state two-surface plasticity model for sands', *Geotechnique*, **47** (2), 255–272 (1997).
8. K. Been, J. H. A. Crooks, D. E. Becker and M. G. Jefferies, 'The cone penetration test in sands: Part I, state parameter interpretation', *Geotechnique*, **36,** 239–249 (1986).
9. J. A. Sladen, 'Discussion: Cone penetration test calibration for Erksak sand', *Can. Geotech. J.*, **26,** 173–177 (1988).
10. J. A. Sladen, 'Problems with interpretation of sand state from cone penetration test', *Geotechnique*, **39,** 323–332 (1989).
11. R. F. Bishop, R. Hill and N. F. Mott, 'Theory of indentation and hardness tests', *Proc. Phys. Soc.*, **57,** 147–159 (1945).
12. R. Hill, 'The mathematical theory of plasticity', Oxford University Press, Oxford, 1950.
13. Chadwick, 'The quasi-static expansion of a spherical cavity in metals and ideal soils', *Q. J. Mech. Appl. Math.*, **12,** 52–71 (1959).
14. J. P. Carter, J. R. Booker and S. K. Yeung, 'Cavity expansion in cohesive frictional soils', *Geotechnique*, **36** (3), 349–358 (1986).
15. H. S. Yu and G. T. Houlsby, 'Finite cavity expansion in dilatant soils: loading analysis. *Geotechnique* **41** (2), 173–183 (1991).
16. M. G. Jefferies and K. Been, 'Cone factors in sand', *Proc. CPT'95*, Swedish Geot. Soc., 1995, pp. 187–193.
17. A. N. Schofield and C. P. Wroth, 'Critical state soil mechanics'. London, McGraw-Hill (1968).
18. K. Been, M. G. Jefferies and J. Hachey, 'The critical state of sands', *Geotechnique*, **31** (3), 365–381 (1991).
19. Ishihara, '33rd Rankine lecture—liquefaction and flow failure during earthquakes', *Geotechnique*, **41,** 351–415 (1993).
20. R. Nova, 'A constitutive model for soil under monotonic and cyclic loading', in G. N. Pande and O. C. Zienkiewicz (eds), *Soil Mechanics—Transient and Cyclic Loads*, Wiley, Chichester, 1982, pp. 343–373.
21. D. C. Drucker, R. E. Gibson and D. J. Henkel, 'Soil mechanics and work-hardening theories of plasticity', *J. Soil Mech. Foundation Engng. ASCE*, **122,** 338–346 (1957).
22. F. E. Richart, J. R. Hall and R. D. Woods, *Vibrations of Soils and Foundations*, Prentice-Hall, Englewood Cliffs, NJ, 1970.
23. Pestana and Whittle, 'Compression model for cohesionless soils', *Geotechnique* **45,** 611–631 (1995).
24. R. Bellotti, M. Jamiolkowski, D. C. F., Lo Presti and D. A. O'Neill, 'Anisotropy of small strain stiffness in Ticino sand', *Geotechnique* **46** (1), 115–131 (1996).
25. G. Baldi, R. Bellotti, N. Ghionna, M. Jamiolkowski and E. Pasqualini, 'Interpretation of CPT's and CPTU's', 2nd Part, *Proc. 4th Int. Geot. Seminar*, Nanyang Technological Institute, Singapore, 1986, pp. 143–156.
26. O. C. Zienkiewicz and I. C. Cormeau, 'Viscoplasticity, plasticity and creep in elastic solids. A unified numerical approach', *Int. J. Numer. Meth. Eng.*, **8,** 821–845 (1974).
27. I. M. Smith and D. V., Griffiths, Programming the Finite Element Method, 2nd edn., Wiley, 1988.
28. D. V. Griffiths, 'Finite element analysis of walls, footings and slopes', *Ph.D. Thesis*, University of Manchester, 1980.
29. Yy H-S., Cavity expansion theory and its application to the analysis of pressuremeters. *Ph.D. Thesis*. University of Oxford (1990).
30. O. C. Zienkiewicz and R. L. Taylor, (1991); *The Finite Element Method*, Vol. 2, McGraw-Hill, New York.
31. R. E. Gibson and W. F. Anderson, '*In situ* measurement of soil properties with the pressuremeter', *Civil Engng. Public Works Rev.*, **56** (658), 615–618 (1961).
32. G. T. Houlsby and N. J. Withers, (1988); 'Analysis of the cone pressuremeter in clay', *Geotechnique* **38,** 575–587.
33. D. E. Harman, (1976); 'A statistical study of static cone bearing capacity, vertical effective stress, and relative density of dry and saturated fine sands in a large triaxial testing chamber', *M.Sc. Thesis*, University of Florida, 1976.

